Mixed-Valence, Mixed-Spin-State, and Heterometallic [2×2] Grid-type Arrays Based on Heteroditopic Hydrazone Ligands: Synthesis and Electrochemical Features

Lindsay H. Uppadine,[a] Jean-Paul Gisselbrecht,*[b] Nathalie Kyritsakas,[c] Kalle Nättinen,[d] Kari Rissanen,[d] and Jean-Marie Lehn*[a]

Abstract: An extended family of heterometallic $[M^1{}_2M^2{}_2(L^-)_4]^{n+}$ [2×2] grid-type arrays **1**–**9** has been prepared. The three-tiered synthetic route encompasses regioselective, redox and enantioselective features and is based on the stepwise construction of heteroditopic hydrazone ligands **A**–**C**. These ligands contain ionisable NH and non-ionisable NMe hydrazone units, which allows the metal redox properties to be controlled according to the charge on the ligand binding pocket. The 2-pyrimidine (R) and 6-pyridine (R′) substituents have a significant effect on complex geometry and influence both the electrochemical and magnetic behaviour of the system. ^{1}H NMR spectroscopic studies show that the Fe^{II} ions in the grid can be low spin, high spin or spin crossover depending on the steric effect of substituents R and R′. This steric effect has been manipulated to construct an unusual array possessing two low-spin and two spin-crossover Fe^{II} centres (grid **8**). Electrochemical studies were performed for the grid-type arrays **1**–**9** and their respective mononuclear precursor complexes **10**–**13**. The grids function as electron reservoirs and display up to eight monoelectronic, reversible reduction steps. These processes generally occur in pairs and are assigned to ligand-based reductions and to the Co^{III}/Co^{II} redox couple. Individual metal ions in the heterometallic grid motif can be selectively addressed electrochemically (e.g., either the Co^{III} or Fe^{II} ions can be targeted in grids **2** and **5**). The Fe^{II} oxidation potential is governed by the charge on the ligand binding unit, rather than the spin state, thus permitting facile electrochemical discrimination between the two types of Fe^{II} centre in **7** or in **8**. Such multistable heterometallic [2×2] gridlike arrays are of great interest for future supramolecular devices incorporating multilevel redox activity.

Keywords: cyclic voltammetry · grid-type complexes · hydrazone ligands · spin crossover · supramolecular chemistry

Introduction

A potentially very powerful approach to smart electronic materials relies on the self-organisation of metallosupramolecular complexes demonstrating multistable behaviour.[1] For eventual applications in information storage technology, the multistable system should be addressable by means of an external perturbation (e.g., temperature, pressure or light) and possess a readable response function (such as magnetic susceptibility or optical absorption). The requirement for multistability can be achieved by manipulating a variety of intrinsic molecular features, including redox level,[2] spin state[3] and protonation state.[4] Such switchable molecular or supramolecular domains are often accompanied by hysteresis effects, which confer molecular memory properties on the system.

Gridlike arrays of metal ions are potential candidates for information storage devices, because of their well-defined

[a] Dr. L. H. Uppadine, Prof. J.-M. Lehn
ISIS, Université Louis Pasteur
CNRS UMR 7006, BP 70028, 67083 Strasbourg (France)
Fax: (+33) 390-245-140
E-mail: lehn@isis.u-strasbg.fr

[b] Dr. J.-P. Gisselbrecht
Laboratoire d'Electrochimie et de Chimie-Physique du Corps Solide
UMR 7512, CNRS-Université Louis Pasteur
4 rue Blaise Pascal, 67000 Strasbourg (France)
Fax: (+33) 390-241-431
E-mail: gissel@chimie.u-strasbg.fr

[c] N. Kyritsakas
Institut de Cristallochimie, Institut le Bel
Université Louis Pasteur, 4 rue Blaise Pascal
67000 Strasbourg (France)

[d] Dr. K. Nättinen, Prof. K. Rissanen
NanoScience Center, Department of Chemistry
University of Jyväskylä, P.O. Box 35
40351 Jyväskylä (Finland)

 DOI: 10.1002/chem.200401224

architecture and intriguing physical characteristics.[5] Examples to date illustrate the rich chemistry of this metallosupramolecular motif and include complexes displaying spin-crossover phenomena,[3a,b] antiferromagnetic[6,2e] and ferromagnetic coupling,[6c,7] multilevel redox properties[2a–e] and pH-dependent optical switching.[4a] In particular, heterometallic gridlike arrays promise interesting physicochemical features due to precise positioning of different metallic centres.[2b,c] Thus, information can be written at specific sites in the array by addressing individual metal ions with an external stimulus.[8]

Self-assembly is an invaluable strategy for the synthesis of metallosupramolecular complexes[1a,9] and has proved particularly useful for the preparation of grid-type arrays.[5] This highly convergent approach allows intricate structures to be fabricated without recourse to tedious nanofabrication techniques.[1a] The advantages of metal ions in the self-assembly process are manifold and include 1) a wide range of coordination numbers and geometries, 2) tunable ligand exchange kinetics (e.g., by varying the metal oxidation state), 3) photophysical, magnetic and redox properties, 4) control of assembly–diassembly (e.g., by electrochemical interconversion between different metal oxidation states[10]) and 5) access to chiral assemblies (e.g., for applications in chiral host–guest recognition).

Homometallic [2×2] grids are usually constructed by means of simple high-yielding self-assembly reactions involving the appropriate ditopic ligand and metal ion.[11] In contrast, the synthesis of $[M^1{}_2M^2{}_2L_4]^{n+}$ heterometallic grids requires special procedures, since *anti*- or *syn*-arrangements of the metal ions could theoretically exist.[2b,c] One successful synthetic strategy utilises sequential self-assembly coupled with a protection/deprotection step.[2b,c] Thus, two bis(terdentate) homoditopic ligands can be used to generate a mononuclear "corner complex" $[M^1L_2]^{2+}$ ($M^1 = Ru^{II}$ or Os^{II}), containing two free binding sites. The $[M^1L_2]^{2+}$ complexes are subseqently combined with a second type of metal ion to assemble the heterometallic $[M^1{}_2M^2{}_2L_4]^{8+}$ grid exclusively as the *anti*-topoisomer. These metalloarrays are capable of exhibiting multistable redox behaviour, as exemplified by electrochemical studies of $[Fe_4L_4]^{8+}$, $[Ru_2Os_2L_4]^{8+}$ and $[Ru_2Fe_2L_4]^{8+}$.[2b]

An alternative approach to mixed metal motifs has recently been reported and relies on a *heteroditopic* ligand with an electronically "soft" bidentate site coupled to a "hard" terdentate unit.[12] These binding pockets are programmed to discriminate between metal ions on the basis of preferred coordination geometry and hard/soft nature. A single-step self-assembly reaction with zinc(II) and copper(I) ions affords the [2×2] heterometallic array $[Zn^{II}{}_2Cu^{I}{}_2(L^-)_4]^{2+}$, containing "hard" Zn^{II} octahedrally coordinated by two tridentate units, and "soft" Cu^{I} in a tetrahedral bis(bidentate) pocket.

We now report a novel methodology for the generation of mixed-valence, mixed-spin-state and heterometallic [2×2] grid-type arrays **1**–**9**.[13] The synthetic pathway utilises a three-level strategy involving 1) steric control of regioselectivity, 2) protonic modulation of redox state and 3) chiroselective–toposelective self-assembly. This approach allows two types of octahedral metal centres to be introduced, while circumventing the need for protection/deprotection steps.

The grid scaffold is based on the stepwise construction of heteroditopic ligands **A**–**C** (Scheme 1), composed of both ionisable NH hydrazone and nonionisable NMe hydrazone terdentate sites. This feature allows redox properties to be controlled according to the charge on the ligand binding pocket. The 2-pyrimidine substituent R is sandwiched between two opposing ligands in the grid structure and therefore plays an important role in the overall geometry of the complex. This in turn has significant effects on both the electrochemical and magnetic properties of the system. The R′ group on the grid periphery influences the coordination environment around the metal ion M^2, and is used to tune the spin state when $M^2 = Fe^{II}$ (Scheme 1).

Abstract in French: *Une famille de complexes hétérométalliques $[M^1{}_2M^2{}_2(L^-)_4]^{n+}$ du type grille [2×2] **1–9** a été préparée. Les trois approches synthétiques multiétapes des ligands hydrazone hétéroditopiques **A–C** possèdent chacune des caractéristiques régio-, rédox-, énantio-sélectives. Ces ligands possèdent un groupement NH ionisable et un groupement hydrazone non-ionisable NMe, qui permettent un contrôle des propriétés rédox du métal complexé en fonction de la charge de la cavité coordinante. Les substituants 2-pyrimidine (R) et 6-pyridine (R′) influencent de manière significative la géométrie des complexes formés ainsi que leurs propriétés électrochimiques et magnétiques. Les études par spectroscopie RMN ^1H montrent que les ions Fe^{II}, dans ces complexes, possèdent une configuration électronique soit de bas spin, soit de haut spin ou encore de transition de spin en fonction de l'encombrement stérique du substituant. Cet effet stérique a été utilisé pour construire des grilles originales possédant deux cations Fe^{II} de bas spin et deux cations Fe^{II} à transition de spin (grille **8**). Des études électrochimiques détaillées ont été réalisées pour les assemblages du type grille **1–9** et leurs précurseurs mononucléaires **10–13**. Ces grilles fonctionnent comme réservoir à électrons. Jusqu'à huit étapes de réduction monoélectronique réversibles peuvent être observées. Ces transferts d'électrons se font généralement par paire et interviennent sur le ligand à l'exception des deux premières réductions correspondant aux couples Co^{III}/Co^{II}. Chaque cation métallique d'une grille peut être sollicité sélectivement par voie électrochimique (les ions Co^{III} ou Fe^{II} peuvent être ciblés dans les grilles **2** et **5**). Le potentiel d'oxydation du Fe^{II} est tributaire de la charge des ligands et non de l'état de spin, permettant une discrimination électrochimique parmi les deux types de Fe^{II} dans **7** ou **8**. De telles grilles [2×2] hétérométalliques ont des niveaux de stabilité multiples et présentent un grand intérêt pour des systèmes supramoléculaires possédant une multiplicité de niveaux d'oxydo-réduction.*

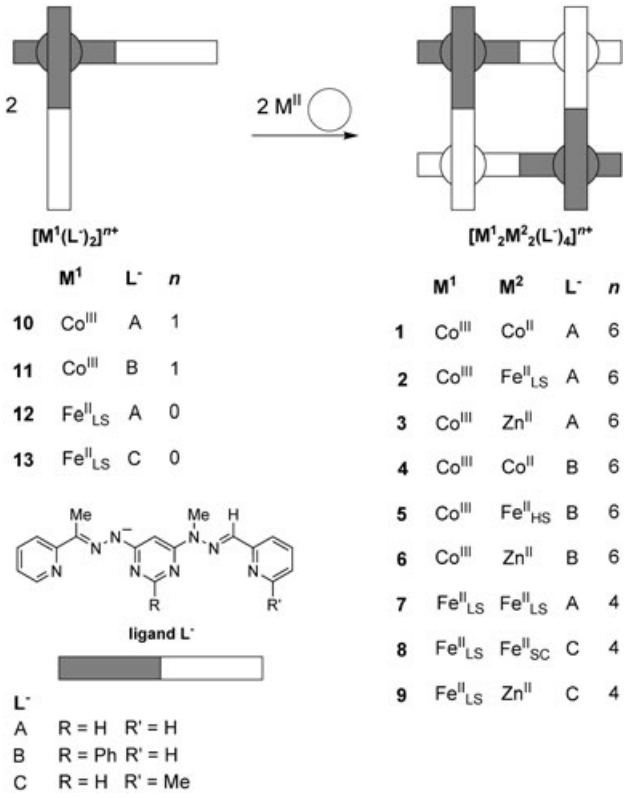

Scheme 1. Self-assembly of the heterometallic [2×2] grid-type arrays **1**–**9** from the corner complexes $[M^1(L^-)_2]^{n+}$ ($M^1=Co^{III}$, $n=1$; $M^1=Fe^{II}$, $n=0$). (HS, LS and SC designate high spin, low spin and spin crossover, respectively.)

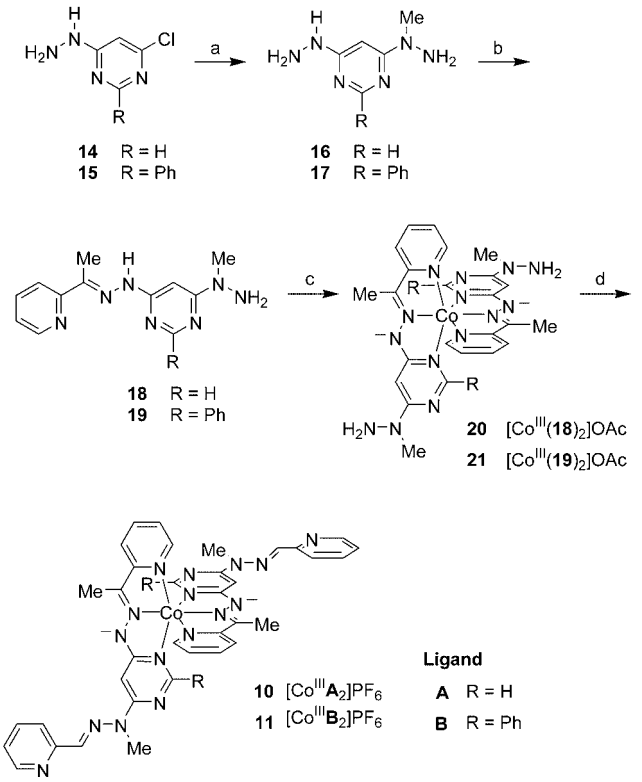

Scheme 2. Synthesis of the cobalt(III) corner complexes **10**,**11**. a) $MeNHNH_2$, MeOH; b) 2-acetylpyridine, MeOH; c) $Co^{II}(OAc)_2\cdot 4H_2O$, MeOH (**20**) or H_2O:MeOH (7:3 v/v) (**21**); d) 2-pyridinecarboxaldehyde, MeOH (**10**) or H_2O:MeOH (7:3 v/v) (**11**), then NH_4PF_6(aq).

The monometallic corner complexes **10**–**13** were constructed by using cobalt(III) or iron(II) ions (Scheme 1). These metals were selected in order to prepare grids with a $Co^{III}_2Co^{II}_2$ mixed-valence structure (grids **1** and **4**), or a mixed-spin-state $(Fe^{II}_{LS})_2(Fe^{II}_{SC})_2$ composition (grid **8**; LS = low spin, SC = spin crossover). To complete the series, we also synthesised grid systems based on $Co^{III}_2Fe^{II}_2$, $Co^{III}_2Zn^{II}_2$, $(Fe^{II}_{LS})_2(Fe^{II}_{LS})_2$ and $(Fe^{II}_{LS})_2Zn^{II}_2$ heterometallic motifs. This extended family reveals correlations between the physical properties of the metalloarray and the type of primary metal ion M^1, secondary metal M^2 and ligand substituents R/R′. We describe here the synthetic approach to the heterometallic complexes, together with an in-depth analysis of their electrochemical behaviour.

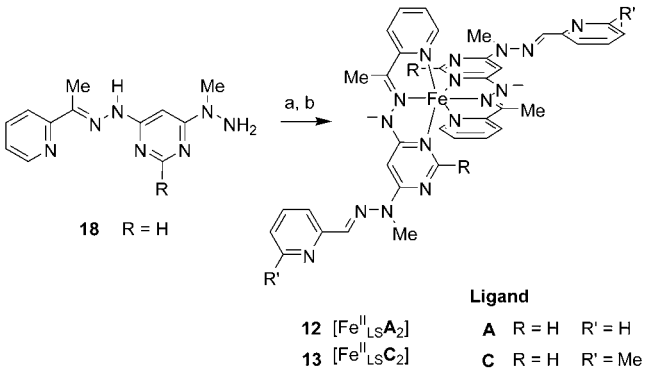

Scheme 3. Synthesis of the iron(II) corner complexes **12**,**13**. a) $Fe(BF_4)_2\cdot 6H_2O$, MeOH; b) 2-pyridinecarboxaldehyde, MeOH, then Al_2O_3 (1:1 CH_2Cl_2/MeCN) (**12**); 6-methyl-2-pyridinecarboxaldehyde, MeOH, then Al_2O_3 (2:1 CH_2Cl_2/MeCN) (**13**).

Results and Discussion

Synthesis of the heterometallic [2×2] grid-type complexes: The key intermediates in the synthesis of the [2×2] grid arrays **1**–**9** are the cobalt(III) and iron(II) corner complexes **10**–**13** (Scheme 1). A stepwise route was used to prepare these complexes, as illustrated in Schemes 2 and 3.

Both the cobalt(III) and iron(II) corner complexes are constructed with terdentate ligands containing only one metal binding site (compounds **18** or **19**, Schemes 2 and 3). These ligands were prepared by a regioselective synthetic approach, as outlined in Scheme 2. Thus, 4-chloro-6-hydrazinopyrimidine (**14**)[14] or 4-chloro-6-hydrazino-2-phenylpyrimidine (**15**)[15] were reacted with *N*-methylhydrazine to yield compounds **16** and **17**, respectively, which were subsequently condensed with one equivalent of 2-acetylpyridine (Scheme 2). The condensation reaction occurs at the

$NHNH_2$ site rather than the $MeNHNH_2$ site of **16**,**17** to afford ligands **18**,**19**, respectively. This site selectivity avoids an unfavourable 1,3-steric interaction between the methyl groups of **16** or **17** and the 2-acetylpyridine reagent.

The route to cobalt(III) complexes **10**,**11** uses the ionisable NH hydrazone sites of **18**,**19** to promote a redox reaction at the metal centre (Scheme 2). Thus, $Co^{II}(OAc)_2 \cdot 4H_2O$ reacts with **18**,**19** to afford the deprotonated Co^{III} complexes **20** and **21**, respectively. This reaction depends on a synergistic coupling between the deprotonation of ligands **18**,**19** by the AcO^- ion, and the aerial oxidation of Co^{II} to the +3 oxidation state, which is stabilised by two negatively charged ligands.[16]

Condensation of complexes **20**,**21** with 2-pyridinecarboxaldehyde generates the corner complexes **10**,**11** that contain two additional binding pockets (Scheme 2). These sites are constructed from neutral hydrazone units, which cannot be deprotonated because the hydrazone group is protected by *N*-methylation. This enables cobalt(II) ions to be introduced at the neutral sites without further oxidation to cobalt(III).

The cobalt(III) centres in **10**,**11** are inert towards substitution; this prevents scrambling when a second metal is added to assemble the grid (Scheme 1). As previously discussed, this last step is enantioselective, because the grid array can only be constructed from two corner complexes of the same chirality (e.g., (*R*)-**10** + (*R*)-**10**, but not (*R*)-**10** + (*S*)-**10**).[2c,13]

Three types of secondary metal ion M^2 (Zn^{II}, Co^{II}, Fe^{II}) were employed to assemble the target [2×2] grid arrays $[Co^{III}{}_2M^2{}_2(L^-)_4]^{6+}$ **1**–**6** (Scheme 1). The self-assembly reaction was performed by stirring the M^2 ion (as its hydrated BF_4^- salt) with Co^{III} complexes **10** or **11** in acetonitrile, either at room temperature or at reflux. For example, the room-temperature reaction between complexes **10**,**11** and $Co(BF_4)_2 \cdot 6H_2O$ in acetonitrile generated mixed-valence complexes **1** and **4**, respectively. These complexes were recrystallised from $MeCN/Et_2O$ as mixed hexafluorophosphate tetrafluoroborate salts in yields of 75% (**1**) and 67% (**4**).

The second type of grid motif (**7**–**9**) is based on the low-spin iron(II) corner complexes **12** and **13** (Scheme 1). The approach to these grid arrays is similar to the cobalt(III)-containing systems, but with subtle changes in the structural design and synthetic strategy. The main goal was to adapt the synthetic route to afford a grid complex containing Fe^{II} ions in two different spin states, with a view to studying the magnetic properties of the system. To this end, the heteroditopic ligand **C** was designed as a suitable scaffold for a mixed-spin-state $(Fe^{II}{}_{LS})_2(Fe^{II}{}_{SC})_2$ grid (Scheme 1). Ligand **C** possesses two types of site: 1) a deprotonated terdentate unit with no bulky substituents α to the coordinating nitrogen atoms and 2) a neutral binding site with a methyl group (R′) α to the pyridine nitrogen. Metal scrambling should be prevented during the final self-assembly stage (Scheme 1), since the corner complex **13** can be constructed with Fe^{II} strongly coordinated at site 1.[17]

The route to iron(II) corner complex **13** is illustrated in Scheme 3. Ligand **18** is coordinated to iron(II) by reaction with $Fe^{II}(BF_4)_2 \cdot 6H_2O$ in MeOH, and the mononuclear complex is then condensed with 6-methyl-2-pyridinecarboxaldehyde to afford two additional binding sites. The crude red product is simultaneously purified and deprotonated by means of column chromatography on alumina (eluent: 2:1 $CH_2Cl_2/MeCN$), to give the green neutral complex **13** (47% yield based on **18**).[18,19] The ^1H NMR spectrum of **13** in $CDCl_3$ was assigned by a combination of COSY and NOESY experiments and is consistent with a fully deprotonated, diamagnetic (low-spin Fe^{II}) complex. The Fe^{II} site in **13** is stable with respect to aerial oxidation, in contrast to the proton-coupled electron-transfer reaction (PCET) seen for $Co^{II}(OAc)_2$ and ligands **18**–**19**.[20] Unfortunately, attempts to synthesise the Fe^{II} analogue of $[Co^{III}\mathbf{B}_2]^+$ were unsuccessful, since the iron(II) complex of ligand **B** decomposes on alumina. This may be due to the destabilising steric effect of the phenyl group, which is in the α-position relative to the donor pyrimidine nitrogen atom.

The $[(Fe^{II}{}_{LS})_2(Fe^{II}{}_{SC})_2\mathbf{C}_4]^{4+}$ grid **8** is assembled by heating complex **13** and $Fe^{II}(BF_4)_2 \cdot 6H_2O$ in MeCN at reflux temperature (Scheme 1). The ^1H NMR spectrum of the product at 298 K (400 MHz, $[D_3]MeCN$) clearly illustrates the presence of two types of iron(II) spin state: a diamagnetic site and a paramagnetic centre (vide infra). The $[(Fe^{II}{}_{LS})_2Zn^{II}{}_2\mathbf{C}_4]^{4+}$ grid **9** was prepared in an analogous fashion from complex **13** and zinc(II). This grid system is fully diamagnetic and serves as a useful reference for grid **8** in the ^1H NMR spectroscopic and electrochemical studies.

The effect of ligand structure on iron(II) spin state was confirmed by preparing the tetrairon(II) grid based on ligand **A** (R′ = H, Scheme 1). Thus, self-assembly of $[Fe^{II}{}_{LS}\mathbf{A}_2]$ (**12**) and $Fe^{II}(BF_4)_2 \cdot 6H_2O$ in MeCN generates grid **7** containing four low-spin iron(II) centres (vide infra).

X-ray crystallographic studies: Crystals of the corner complex $[Co^{III}\mathbf{A}_2]PF_6$ (**10**) were grown from $Et_2O/MeCN$ and characterised by X-ray crystallography (Figures 1 and 2). As seen from Scheme 1, ligand **A** possesses both neutral and negatively charged terdentate binding pockets. The crystal structure of complex **10** shows that only the negatively charged site of each ligand coordinates to the cobalt(III) centre, leaving two free metal binding sites per complex. The Co^{III} ion exhibits distorted octahedral coordination (average N_{pyr}-Co-N_{pym} bite angle = 164.2°), provided by two pyridine (d_{Co-N} = 1.932, 1.929 Å), two pyrimidine (d_{Co-N} = 1.917, 1.909 Å) and two hydrazone nitrogen atoms (d_{Co-N} = 1.879, 1.858 Å). Thus, the axial Co–N bond lengths to the hydrazone donor atoms are shorter than the Co–N distances to the equatorially coordinated pyrimidine and pyridine rings. These bond lengths are roughly consistent with the average axial and equatorial Co–N bond lengths found for $[Co^{III}(terpy)Cl_3(H_2O)_{11}]$ (d_{Co-N} = 1.859 (ax), 1.928 Å (eq)).[21] The metal-free terdentate binding sites (defined by N25, N27, N28 and N5, N7, N8, respectively) display different conformations from the two sites coordinated to Co^{III} (N1, N2, N4 and N21, N22, N24). This is due to the strong preference for *anti*-conformations for N5–N7, N7–N8, N25–N27 and N27–N28.[22]

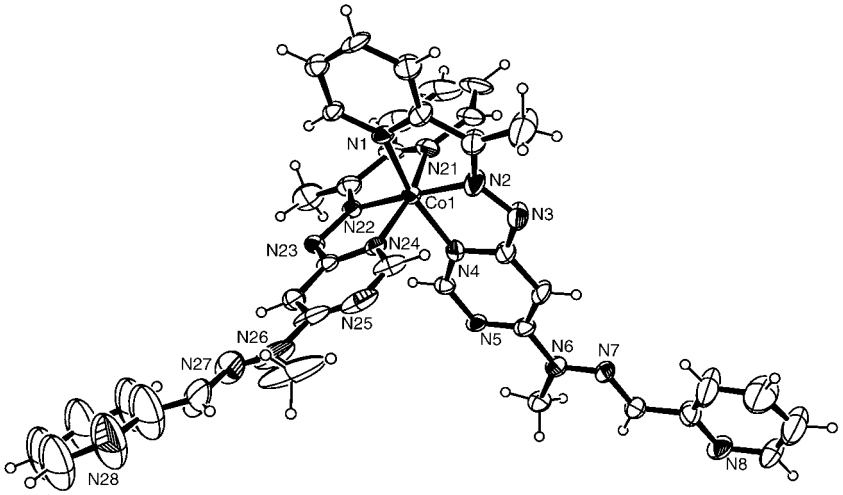

Figure 1. Solid-state structure of cobalt(III) corner complex **10** (single molecule plot with thermal ellipsoids).

spontaneous resolution of the enantiomers has occurred and all the complexes have the same handedness.[24] A probable reason for this phenomenon is the packing of the molecules into a curved tetrameric structure.

Crystals of the heterometallic [2×2] grid-type array $[Co^{III}_2Zn^{II}_2\mathbf{B}_4](PF_6)_3(BF_4)_3$ (**6**) were obtained from Et_2O/MeCN and the structure was determined by X-ray crystallography (Figure 3). The complex cation consists of an approximately square array of alternating cobalt(III) and zinc(II) ions (average inner angles: Zn-Co-Zn = 84.5°, Co-Zn-Co = 95.6°), with each metal displaying distorted octahedral coordination to two perpendicularly oriented ligand fragments. The

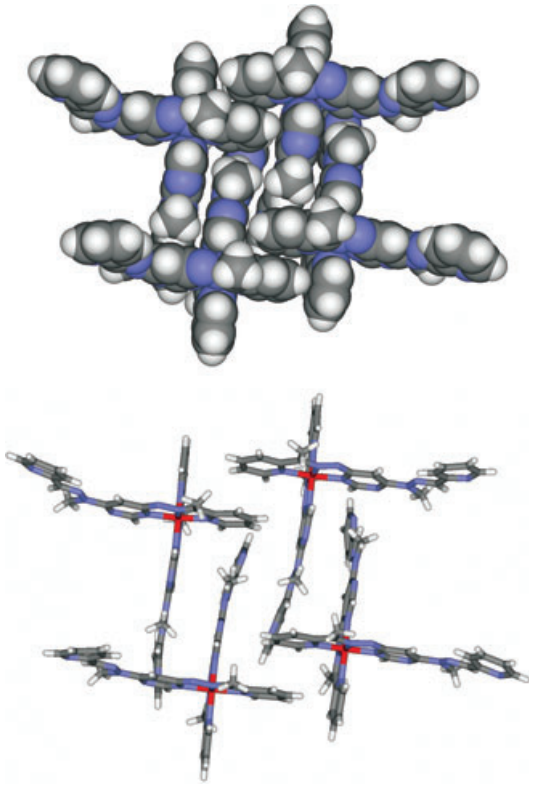

Figure 2. Packing plot for the solid-state structure of cobalt(III) corner complex **10**, illustrating the π–π assembled curved tetramer (space filling and stick representations, top and bottom, respectively).

Four complex molecules **10** assemble through a series of π–π interactions to generate a curved tetrameric structure in the solid state (Figure 2). This interdigitation of ligand planes is reminiscent of the well-known edge-to-face and offset-face-to-face interactions that occur between the outer pyridine rings in many $[M(terpy)_2]^{n+}$ complexes.[23] Since compound **10** crystallises in the acentric space group $I\bar{4}2d$, a

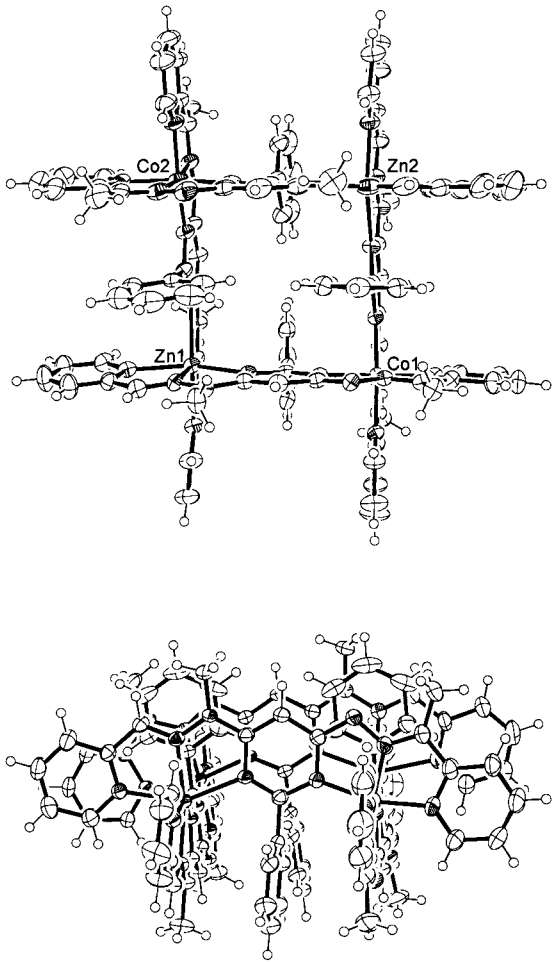

Figure 3. Top and side views of the solid-state structure of [2×2] grid array $[Co^{III}_2Zn^{II}_2\mathbf{B}_4](PF_6)_3(BF_4)_3$ (**6**) (50% thermal ellipsoids).

Co–N bond lengths fall into three groups according to the type of donor N atom, with the shortest distances between Co^{III} and the hydrazone moieties (pyridine $d_{Co-N}=1.942$–1.955 Å; pyrimidine $d_{Co-N}=1.974$–1.991 Å; hydrazone $d_{Co-N}=$ 1.874–1.888 Å). The Zn–N bond lengths are significantly longer than the Co–N bonds, reflecting weaker coordinative interactions at the d^{10} zinc(II) centre compared to the low-spin d^6 cobalt(III) ion (pyridine $d_{Zn-N}=2.186$–2.196 Å; pyrimidine $d_{Zn-N}=2.193$–2.233 Å; hydrazone $d_{Zn-N}=2.098$–2.147 Å). Interestingly, slow crystallisation over a period of two weeks generated crystals with three PF_6^- and three BF_4^- counterions; the complex was originally prepared as the bis(hexafluorophosphate) tetrakis(tetrafluoroborate) salt from $[Co^{III}\mathbf{B}_2]PF_6$ and $Zn^{II}(BF_4)_2$.

The [2×2] grid complex $[Fe^{II}_2Zn^{II}_2\mathbf{C}_4](BF_4)_4$ (**9**) was crystallised from $Et_2O/MeNO_2$ and its structure investigated by X-ray diffraction (Figure 4). The cation possesses the anticipated grid-type array of alternating iron(II) and zinc(II) ions, each coordinated in a distorted N_6 octahedral environment by two mer-N_3 donor sets from a pair of perpendicularly oriented ligands. The iron(II) coordination site shows a marked tetragonal distortion and displays shorter Fe–N bonds to the hydrazone moieties relative to the pyridine and pyrimidine rings (hydrazone $d_{Fe-N}=1.895$–1.906 Å; pyridine $d_{Fe-N}=$ 1.934–1.957 Å; pyrimidine $d_{Fe-N}=1.933$–1.971 Å). These distances are comparable to the Fe–N bond lengths in low-spin iron(II) terpyridine complexes and therefore confirm the low-spin assignment for the two iron(II) centres.[25] As expected, the Zn–N bond lengths are significantly longer than the Fe–N distances (hydrazone $d_{Zn-N}=2.161$–2.162 Å; pyridine $d_{Zn-N}=2.182$–2.205 Å; pyrimidine $d_{Zn-N}=2.128$–2.137 Å). The longest Zn–N bond lengths correspond to the 6-methyl-substituted pyridine rings, since the methyl group presents a steric barrier to coordination and prevents close approach of the pyridine donor atom to zinc(II).[26] This attenuates the ligand field and explains why the Zn^{II} centres can be substituted by Fe^{II} ions that exhibit thermally induced spin crossover (grid **8**). The four ligands divide into two sets, with one pair situated above and the other below the $Fe^{II}_2Zn^{II}_2$ mean plane. Viewed from the centre of the grid, the first two ligands are concave (centroid–centroid distances between two pyrimidine rings or an unsubstituted pyridine and a 6-methylpyridine ring = 5.48, 4.86, 4.88 Å, respectively), and are canted towards each other. The remaining two ligands are convex (centroid–centroid distances between two pyrimidine rings or an unsubstituted pyridine and a 6-methylpyridine ring = 4.82, 6.19, 6.19 Å, respectively), and are tilted away from each other. In contrast, the ligands are nearly parallel within each pair in the solid-state structure of $[Co^{III}_2Zn^{II}_2\mathbf{B_4}](BF_4)_3(PF_6)_3$ (**6**) (centroid–centroid distances between two pyrimidine or two pyridine rings = 6.36, 6.44, 6.74 Å (pair 1); 6.36, 6.43, 6.46 Å (pair 2)). This is due to the 2-pyrimidine phenyl substituent in **6** (absent in **9**), which inserts between two parallel ligands and stabilises the structure through π–π stacking interactions.

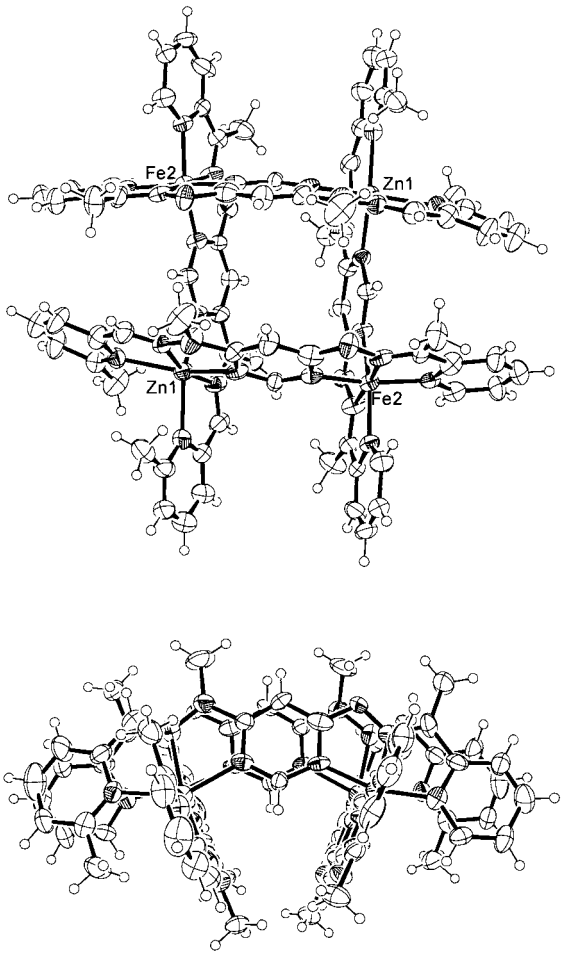

Figure 4. Top and side views of the solid-state structure of [2×2] grid array $[Fe^{II}_2Zn^{II}_2\mathbf{C}_4](BF_4)_4$ (**9**) (50% thermal ellipsoids).

^{1}H NMR spectroscopy: Both the nature of the R group at the pyrimidine 2-position and the type of secondary metal ion M^2 have a profound influence on the magnetic properties of the Co^{III}-based grids **1**–**6**. The magnetic features can be investigated in solution by means of ^{1}H NMR spectroscopy, and a preliminary discussion of the results for grids **1**–**3** has already been presented.[13] The ^{1}H NMR spectra of mixed-valence grids **1** and **4** were analysed by two-dimensional experiments (COSY and ROESY) and the proton T_1 relaxation times were recorded. These grid complexes exhibit similarities in their ^{1}H NMR spectra: 1) both display a set of broad, paramagnetically shifted peaks over a large chemical shift range ($\delta=207$ ppm (**1**), 250 ppm (**4**)), attributed to the influence of the paramagnetic Co^{II} ion on the local magnetic field and proton relaxation rate;[27,28] 2) both possess a set of five sharper peaks in the region 0–15 ppm, assigned to the pyridyl and methyl protons adjacent to the diamagnetic Co^{III} centre. In addition, five distinct signals are observed for the phenyl protons in **4**, indicating that rotation about the pyrimidine–phenyl bond is sterically hindered in the complex.[29] In contrast, the $Co^{III}_2Zn^{II}_2$-based complexes **3** and **6** both contain four diamagnetic metal centres and

therefore display diamagnetic ^{1}H NMR spectra over a limited chemical shift range of approximately 5.5 ppm.

The $Co^{III}_2Fe^{II}_2$ complex **2** (R = H) also possesses a diamagnetic ^{1}H NMR spectrum, signifying that the two iron(II) centres are in the low-spin state. However, introduction of a phenyl group at the pyrimidine 2-position generates a grid complex that contains two high-spin iron(II) sites. Literature precedents reveal a variety of factors that can be used to determine the iron(II) spin state, including 1) inter- and intraligand steric effects,[25a,26,30] 2) electronic effects of ligands and their substituents,[31] 3) the ligand protonation state[32] and 4) the type of counterion.[33] For example, both the complex stability and spin state of iron(II) polyimine complexes are influenced by the steric effect of substituents α to the donor nitrogen atoms. A clear demonstration of this phenomenon occurs with tris(1,10-phenanthroline)iron(II) compounds: the unsubstituted phenanthroline complex is low spin, the tris(2-methyl-1,10-phenanthroline) version is less stable and exhibits spin crossover, while the tris(2,9-dimethyl-1,10-phenanthroline) complex is high spin.[26,30a] This behaviour is attributed to the steric effect of methyl groups adjacent to the donor nitrogen atoms, which weakens the Fe^{II}–N coordinative interactions and makes the high-spin state more thermally accessible. The correlation between spin state and 2-pyrimidine substituent has previously been noted for $[Fe^{II}_4L_4]^{8+}$ [2×2] grid complexes (L = 4,6-bis(2′,2″-bipyrid-6′-yl)pyrimidine and derivatives), and is ascribed to a steric effect that distorts the iron(II) coordination sphere.[3b] Variable-temperature experiments performed on **5** (2:1 $[D_3]$MeCN/$[D_6]Me_2CO$, 338–203 K) show that iron(II) remains high spin over the entire temperature range.

The tetrairon(II) grid **8** possesses two types of binding site: a pocket formed by negatively charged ligand units and a neutral site possessing sterically bulky methyl groups α to the donor pyridine nitrogen atoms. Both steric and electronic factors therefore suggest a strongly bound, low-spin Fe^{II} centre at the first site, and a more weakly bound, high-spin or spin-crossover complex at the second site. Figure 5 illustrates the ^{1}H NMR spectrum of grid **8** at 343 K and 298 K ($[D_3]$MeCN) and at 213 K (2:1 $[D_3]$MeCN/$[D_6]Me_2CO$). At 298 K, the complex displays two sets of signals that can be attributed to protons adjacent to the diamagnetic and paramagnetic Fe^{II} sites, respectively. The protons surrounding the paramagnetic Fe^{II} centre are broadened and paramagnetically shifted up to 48 ppm. In contrast, the four relatively sharp pyridyl peaks at the low-spin site occur in the "diamagnetic region" at $\delta = 7.1$ (pyr4), 6.9 (pyr6), 5.9 (pyr3) and 5.7 ppm (pyr5). The spectrum expands to 88 ppm upon heating to 343 K, while a contraction of the spectroscopic window is observed upon cooling the sample. In fact, the ^{1}H NMR spectrum at 213 K does not extend above 10 ppm and is almost completely diamagnetic, suggesting that all four iron(II) sites are in the low-spin state. Thus, ^{1}H NMR solution studies show spin crossover occurring selectively at the Fe^{II} centres coordinated to neutral, sterically hindered terdentate sites. Detailed solid-state magnetic studies of grid **8** are in progress and will be reported elsewhere.[34] As expected, diamagnetic complexes are obtained by replacing the spin-crossover Fe^{II} ions by Zn^{II} (to give grid **9**), or removing the steric effect of the methyl groups R′ (to afford low-spin tetrairon(II) grid **7**, R′ = H).

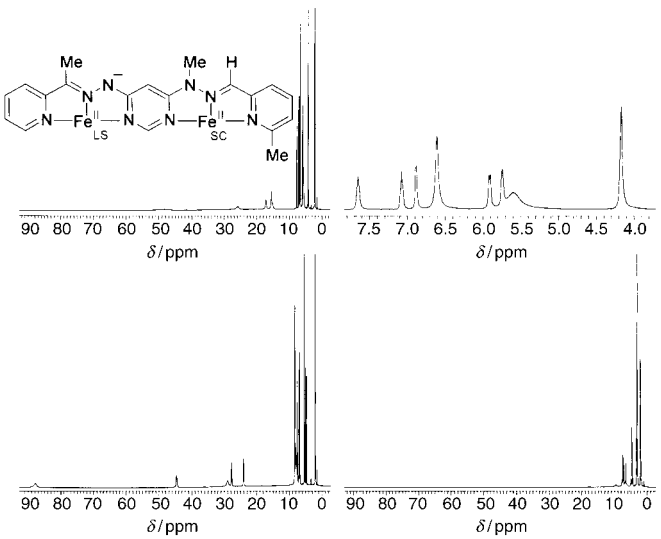

Figure 5. ^{1}H NMR spectra (400 MHz) of grid complex **8**: 298 K, $[D_3]$MeCN, full spectrum (top left); 298 K, $[D_3]$MeCN, high field region (top right); 343 K, $[D_3]$MeCN, full spectrum (bottom left); 213 K, 2:1 $[D_3]$MeCN/$[D_6]Me_2CO$, full spectrum (bottom right). ($[D_6]$Acetone was added to obtain spectra at temperatures below the freezing point of $[D_3]$MeCN at 228 K.)

Electrochemical studies: The redox behaviour of corner complexes **10**–**13** and grid arrays **1**–**9** was investigated in acetonitrile/0.1 M Bu_4PF_6 by using a variety of electrochemical techniques, including cyclic voltammetry, square-wave voltammetry, rotating-disk voltammetry and spectroelectrochemistry. The redox properties of neutral corner complexes **12**,**13** were analysed in dichloromethane for solubility reasons. Most of the grid arrays gave well-defined cyclic voltammograms showing pairs of overlapping one-electron transfers (see Experimental Section and Figure 8 later). Analysis of peak shapes and characteristics with scan rate shows that the first reduction is composed of two overlapping reversible reduc-
tion waves separated by 40–70 mV. The remaining electron transfers have either similar characteristics to the first reduction, or can be resolved as two one-electron transfers, indicative of redox potential differences higher than 70 mV. Table 1 summarises the redox behaviour of the $[Co^{III}(L^-)_2]^+$ precursors **10** and **11** and the corresponding grid complexes **1**–**3** and **4**–**6**, respectively. The data for iron(II) corner complexes **12**,**13** and associated grids **7**–**9** are collected in Table 2. The redox potentials of all complexes are displayed graphically in Figure 6.

*Reduction processes for cobalt(III) corner complexes **10**,**11** and grid arrays **1**–**6***: The cobalt(III) corner complexes **10**,**11** each display two one-electron reversible reduction steps.

Table 1. Redox potential E [V] of corner complexes **10**,**11** and grid complexes **1–6** in MeCN (0.1 M Bu_4NPF_6, glassy carbon electrode, versus Fc^+/Fc, scan rate 0.1 $V s^{-1}$).

	10	**11**	**1**	**2**	**3**	**4**	**5**	**6**
E_{ox} [V][a]	+0.82[b,d]	+1.22[g]	+0.31[g]	+0.92	+1.30[c,d]	+1.46[b]	+1.46[f]	+1.34[b,d]
		+0.98[g]	+0.27[g]	+0.85		+1.14[b,d]	+0.97	+1.18
		+0.73[b,d]					+0.89	+1.12
E_{red} [V][a]	−1.07	−0.84	−0.63	−0.61	−0.65	−0.38	−0.38	−0.40
	−1.98	−1.93	−0.71	−0.70	−0.74	−0.45	−0.44	−0.46
			−1.18	−1.54	−1.60	−1.31	−1.44	−1.60
			−1.27	−1.61	−1.67	−1.37	−1.50	−1.66
			−1.84	−1.80[b,e]		−1.83	−1.78	−1.84
			−1.90			−1.91	−1.87	−1.97
			−2.20[b,e]				−2.20	−2.17
							−2.29	−2.25

[a] One-electron process unless otherwise stated. [b] Two-electron process. [c] Four-electron process. [d] Irreversible oxidation: anodic peak potential. [e] Irreversible reduction: cathodic peak potential. [f] Electrode inhibition. [g] Small amplitude signal.

Table 2. Redox potential E [V] of corner complexes **12**,**13** in CH_2Cl_2 and grid complexes **7–9** in MeCN (0.1 M Bu_4NPF_6, glassy carbon electrode, versus Fc^+/Fc, scan rate 0.1 $V s^{-1}$).

	12	**13**	**7**	**8**	**9**
E_{ox} [V][a]	+0.81[d]	+1.03[d,g]	+0.97	+1.77[c,d]	+1.40[c,d]
	−0.29	+0.74[d]	+0.83	+1.08	+0.15
		−0.27	+0.15	+0.93	+0.10
			+0.08	+0.16	
				+0.10	
E_{red} [V][a]	−2.40[c,e]	−2.25	−1.54	−1.30	−1.58
			−1.59	−1.34	−1.62
			−1.83[b,e]	−1.90[b,f]	−1.84[c,e]
				−2.31[b,f]	

[a] One-electron process unless otherwise stated. [b] Two-electron process. [c] Multielectron process: no. of electrons cannot be determined with accuracy. [d] Irreversible oxidation: anodic peak potential. [e] Irreversible reduction: cathodic peak potential. [f] Reversible reduction seen for scan rates $> 2 V s^{-1}$. [g] Small amplitude signal.

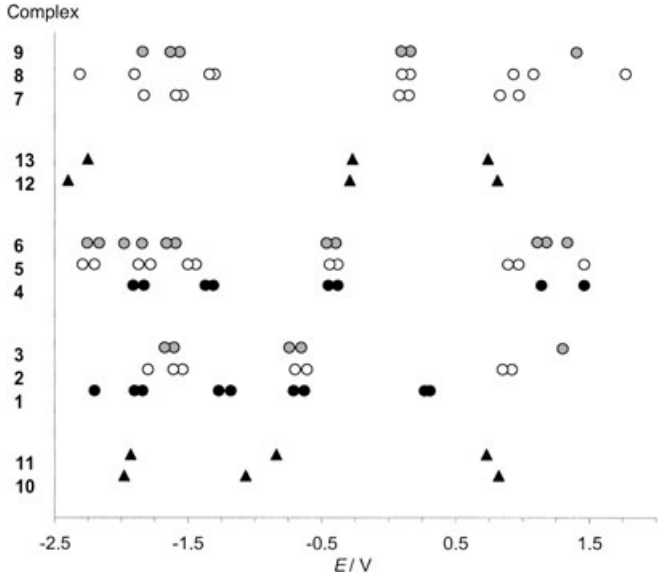

Figure 6. Summary of the redox potentials (E/V) for the redox steps in complexes **1–13**. Corner complexes **10–13** are represented by triangles. The corresponding grid complexes $[Co^{III}{}_2M^2{}_2(L^-)_4]^{6+}$ (**1–6**) or $[(Fe^{II}{}_{LS})_2M^2{}_2(L^-)_4]^{4+}$ (**7–9**) are denoted by circles. Black, white or grey circles correspond to $M^2 = Co^{II}$, Fe^{II} or Zn^{II}, respectively. (Small amplitude signals due to electrogenerated species are omitted for clarity.)

The first reduction process occurs at −1.07 V (**10**) and −0.84 V (**11**), while the second step is observed at significantly more negative potentials (−1.98 V and −1.93 V for **10** and **11**, respectively). Spectroelectrochemical experiments were performed for complex **11** in order to ascertain the site of reduction (Figure 7). The band at 488 nm in the unreduced complex is assigned to a ligand-centred (LC) π–π* transition, since an absorption twice the intensity is observed at 483–485 nm for grids **4–6**, and because bands at 485/495 nm occur in mononuclear cobalt(II) complexes that contain deprotonated pyridylhydrazone li-

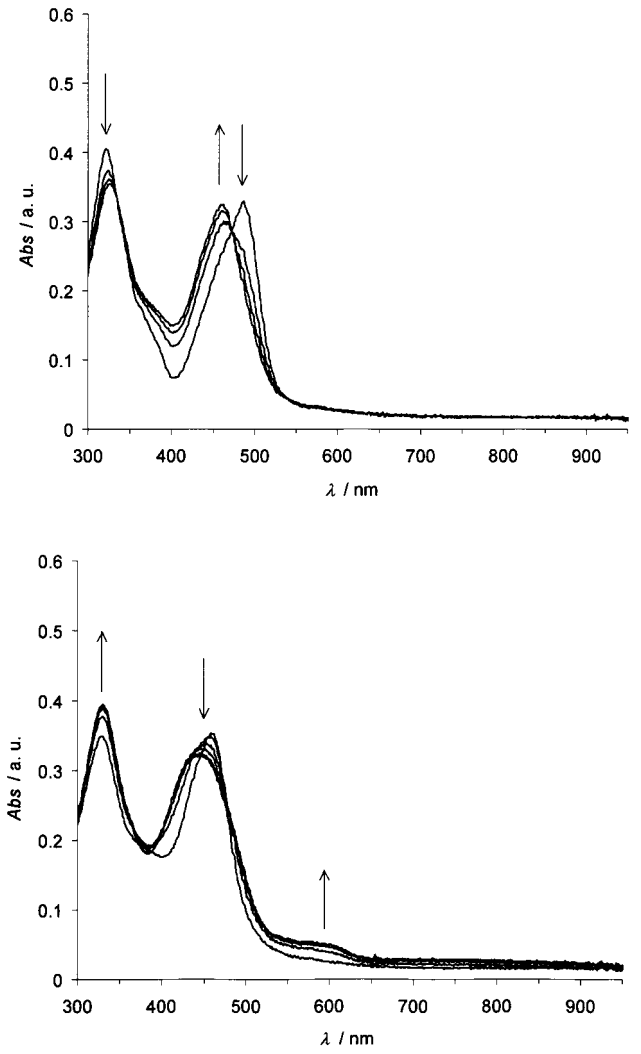

Figure 7. Time-resolved UV-visible spectra for the first (top) and second reduction steps (bottom) of cobalt(III) corner complex **11** in MeCN + 0.1 M Bu_4NPF_6 (spectra recorded every 5 s).

gands.[35] The LC band undergoes a blue shift to 460 nm during the first reduction step, while the absorption at 322 nm decreases and exhibits a small bathchromic shift of 7 nm. The fact that the LC band at 488 nm shifts hypsochromically but retains its intensity suggests that the first reduction is metal-centred. In contrast, a hyperchromic effect is seen for the band at 460 nm during the second reduction step, accompanied by a hypsochromic shift of 16 nm. In addition, a new spectroscopic feature appears around 600 nm, together with a severely broadened absorption extending across the visible and near-IR regions. A decrease of the unreduced ligand π–π* band at 460 nm is predicted if the second reduction is ligand-centred, while the two new low-energy bands are probably intraligand π*–π* transitions from the SUMO of the monoreduced ligand to the first and second ligand-based LUMOs.[36] Similar spectroscopic evolutions were noted for the ligand-based reductions of $[M^{II}_4L_4]^{8+}$ complexes ($M^{II}=Co^{II}$, Fe^{II}; L = 4,6-bis(2′,2″-bipyrid-6′-yl)-2-phenylpyrimidine).[2a]

The cyclic voltammogram of grid **5** is presented as an illustrative example of the reduction behaviour in a $[Co^{III}_2M^2_2(L^-)_4]^{6+}$ grid complex (Figure 8). The site of reduction in these grids was confirmed by spectroelectrochemical investigations similar to those described for complex **11**. The reduction properties of $[Co^{III}_2M^2_2(L^-)_4]^{6+}$ grids (**1**–**6**) display two salient features: 1) an initial pair of overlapping, reversible, one-electron reduction steps occurring on the two Co^{III} centres; 2) one to three pairs of overlapping reversible one-electron reductions at more negative potentials (−1.18 V to −2.29 V), occurring on the ligand (Figure 6, Table 1).

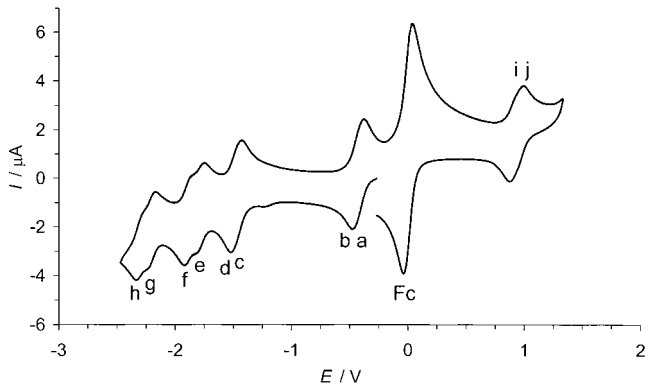

Figure 8. Cyclic voltammogram of $[Co^{III}_2Fe^{II}_2\mathbf{B}_4]^{6+}$ (**5**) + ferrocene in MeCN (0.1 M Bu_4NPF_6, Pt electrode, scan rate 0.1 V s^{-1}, vs Fc/Fc^+). **a**,**b**: Co^{III} reduction; **c**–**h**: ligand reduction; **i**,**j** Fe^{II} oxidation.

Grids **1**–**3** (R = H) exhibit a pair of metal-centred reductions in the range −0.61 V to −0.74 V, while the corresponding values for grids **4**–**6** (R = Ph) appear between −0.38 V and −0.46 V. The cobalt(III) ions are diagonally opposed and therefore too far apart to communicate electronically; this is reflected by the small separation between the two reduction steps (60–90 mV).[37] As expected, the Co^{III}/Co^{II} reduction potentials for grids **1**–**6** are shifted to less negative potentials relative to the mononuclear precursor complexes **10**,**11** ($\Delta E_{1/2}$ = 420–460 mV). Coordination of the metal ion M^2 to the second site of the bridging ligand stabilises the orbitals of the Co^{III} ion, thus facilitating the Co^{III}/Co^{II} reduction process.[2b,38]

The two metal-centred reductions are followed by pairs of ligand-based reduction steps (Figure 6). The separation between the first two ligand-based reductions is typically small ($\Delta E_{1/2}$ = 60–90 mV), indicating that the reduction sites are situated on parallel ligands (average centroid–centroid distance for parallel pyrimidine rings in **6** = 6.35 Å; Figure 3). It should be noted that the reduction potential depends on both the secondary metal ion M^2 and the 2-pyrimidine substituent. For example, the redox potentials are more positive for the first two ligand-based reductions when $M^2=Co^{II}$ rather than Fe^{II} or Zn^{II}, indicating that the metal ion M^2 has a significant effect on the ligand-based LUMOs. Similarly, the first reduction potential is less negative for $[Co^{II}(tpy)_2]^{2+}$ complexes relative to $[Fe^{II}(tpy)_2]^{2+}$ (tpy = 2,2′:6′,2″-terpyridine and derivatives).[39]

A second pair of reversible monoelectronic ligand-based reductions is observed for grids **1** and **4**–**6** (−1.78 V to −1.97 V, Figure 6). Again, the two redox steps occur in close proximity and are assigned to reduction of the second set of parallel ligands in the complex. There is a substantial potential shift between the first and second pairs of ligand-based reductions, which varies in magnitude according to the type of metal ion M^2. Thus, large potential shifts of 570 mV (**1**) and 460 mV (**4**) separate the second and third monoelectronic ligand-based reductions when $M^2=Co^{II}$, while $\Delta E_{1/2}$ spans 280 mV for grid **5** ($M^2=Fe^{II}$) and only 180 mV for **6** ($M^2=Zn^{II}$).

Only grids **5** and **6** display a third pair of reversible one-electron ligand-based reductions (−2.17 V to −2.29 V, Figure 6). This redox behaviour is assigned to further reduction of two already dianionic parallel ligands, with negligible interaction across the grid.

*Oxidation processes for cobalt(III) corner complexes **10**,**11** and grid arrays **1**–**6***: Irreversible oxidation processes have previously been noted for keto–aryl and keto–steroid hydrazones, whereby loss of two electrons and a proton from the hydrazone group generates a reactive intermediate susceptible to nucleophilic attack.[40] The cyclic voltammograms of cobalt(III) corner complexes **10** and **11** also display an irreversible two-electron oxidation step (+0.82 V and +0.73 V, respectively), attributed to the negatively charged hydrazone moiety.

The $[Co^{III}_2Fe^{II}_2(L^-)_4]^{6+}$ grids **2** and **5** both exhibit a pair of reversible, overlapping, one-electron oxidation processes centred around +0.9 V, assigned to Fe^{III}/Fe^{II} redox couples on noninteracting iron centres. The average oxidation potential is only slightly more positive when the Fe^{II} ions are in the high-spin state (**5**) relative to the low-spin version in **2** (av $E_{1/2}$(**5**) − av $E_{1/2}$(**2**) = +45 mV). This relative insensitivity to spin state may reflect counterbalancing steric and elec-

tronic effects in **5**. Thus, the phenyl electron-releasing effect would lower the Fe^{II} oxidation potential, while the phenyl steric influence would lengthen the Fe–N bonds relative to **2**, so destabilising Fe^{III} relative to Fe^{II} and raising the oxidation potential.[25a,41]

The oxidation steps in $[Co^{III}{}_2Zn^{II}{}_2L_4{}^{-}]^{6+}$ grids **3** and **6** are assigned to ligand-based oxidations,[42] since the Zn^{II} centres are redox inactive and literature precedents for reversible[43] and irreversible[40] hydrazone-based oxidations are known. The oxidation potentials of $[Co^{III}{}_2Co^{II}{}_2\mathbf{B}_4]^{6+}$ (**4**) are similar to those of **6**, although the irreversible oxidation at +1.14 V results from partial decomposition of the grid complex.

The oxidation of mixed-valence grid **1** is an unusual case. The cyclic voltammogram of this complex exhibits a quasi-reversible small amplitude oxidation signal when the scan rate is 0.1 $V s^{-1}$ ($E_{1/2}$ = +0.29 V). However, the peak amplitude increases on lowering the scan rate and at 20 $mV s^{-1}$ is comparable to the amplitude of each two-electron reduction step. In addition, the peak potential difference $E_{pa}-E_{pc}$ decreases with scan rate. These observations are consistent with a slow electron-transfer process occurring on the two cobalt(II) ions, as confirmed by spectroelectrochemistry. Slow electron-transfer kinetics may result from Co^{II} oxidation accompanied by a spin change from $Co^{II}{}_{HS}$ to $Co^{III}{}_{LS}$.[44,45]

The failure to observe a similar metal-centred oxidation process for **4** is surprising, since both **1** and **4** contain a mixed-valence $Co^{III}{}_2Co^{II}{}_2$ motif. However, no cobalt(II) oxidation was detected for a homometallic $[Co^{II}{}_4L_4]^{8+}$ hydrazone grid under identical experimental conditions (the Co^{II} ions possess the same coordination environment as the Co^{II} centres in **4**).[2d] Electrochemical analysis of dicobalt(II) triple helicates showed that the Co^{III}/Co^{II} oxidation potential depended on steric constraints.[46] Thus, cobalt(II) cannot be oxidised to cobalt(III) when methyl groups are located α to the donor pyridine nitrogen atoms in the helicate. This is because oxidation from $Co^{II}{}_{HS}$ to $Co^{III}{}_{LS}$ would result in a significant Co–N bond contraction (0.19 Å for $[Co(bpy)_3]^{2+}$),[47] which is effectively precluded by the methyl–methyl steric interaction. In contrast, the complex possessing methyl groups β to the pyridine N atoms is less sterically hindered and exhibits a Co^{II} oxidation wave at +0.37 V versus SCE. The absence of a Co^{II} oxidation step in **4** may therefore reflect a phenyl steric effect, which hampers any geometric reorganisation. Ligand-imposed geometric constraints have been shown to affect the oxidation level of tetranuclear manganese and cobalt systems.[48]

*Reduction processes for iron(II) corner complexes **12**,**13** and grid arrays **7**–**9***: The electrochemical data for the iron(II) precursor complexes **12**,**13** and their corresponding grid complexes **7**–**9** are collected in Table 2 and presented schematically in Figure 6. The redox properties of grid **8** are illustrated by the cyclic voltammograms in Figure 9. The corner complexes **12** and **13** both display a reduction step at very negative potentials, assigned to a ligand-based process (by analogy to the second reduction step in cobalt(III) complexes **10**,**11**). It should be noted that the first reduction at −1.07 V in complex **10** and −0.84 V in **11** is absent in **12**,**13**, which strongly supports the Co^{III}/Co^{II} assignment for this step (vide supra).

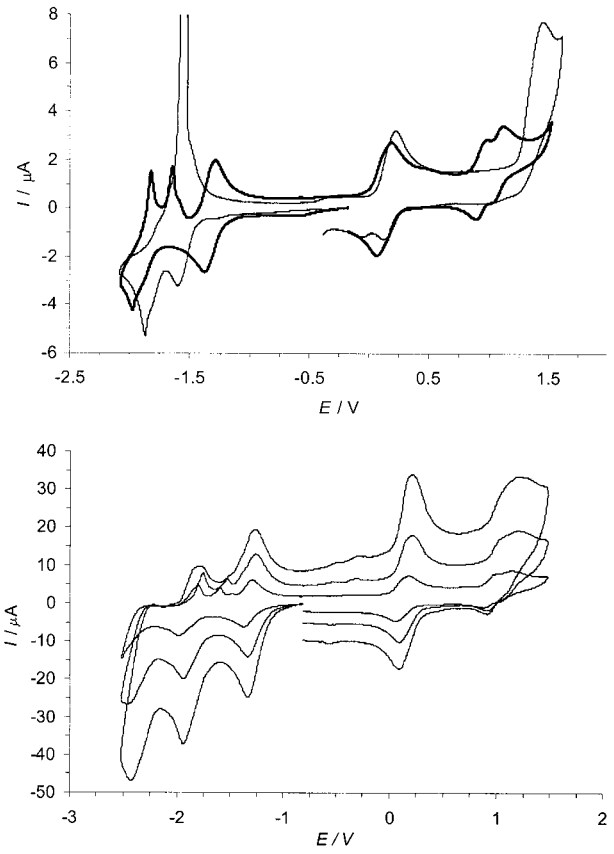

Figure 9. Top: Cyclic voltammograms of grids **8** (bold) and **9** (thin) over the potential range −2.1 V to +1.6 V (MeCN + 0.1 M Bu_4NPF_6, Pt electrode, scan rate 0.1 $V s^{-1}$, vs Fc/Fc^+). Bottom: Effect of scan rate on the cyclic voltammograms of grid **8** (potential range: −2.5 V to +1.48 V vs Fc/Fc^+; scan rate $V^{-1} s^{-1}$ = 5, 2, 0.5; peak amplitude increases with scan rate).

Two ligand-based reduction waves are observed at low scan rates (0.1 $V s^{-1}$) for grids **7**–**9** (Table 2 and Figure 9, top). The first step is reversible and comprises two overlapping monoelectronic reductions at −1.54/−1.59 V (**7**), −1.30/−1.34 V (**8**) and −1.58/−1.62 V (**9**), while the second reduction is irreversible. This latter step yields a deposit on the electrode surface, which is reoxidised on the reverse scan to give sharp peaks characteristic of anodic redissolution processes.

The redox properties of **8** were studied at different scan rates and the cyclic voltammograms are presented in Figure 9 (bottom). When the scan rate is increased above 2 $V s^{-1}$, the second step at −1.90 V becomes reversible and a third reversible reduction is observed at −2.31 V. This reflects the shorter reduction time, which results in a lower concentration of the four-electron reduced species at the electrode surface, thus preventing precipitation at the electrode surface.

*Oxidation processes for iron(II) corner complexes **12**,**13** and grid arrays **7**–**9***: The mononuclear precursor complexes **12** and **13** display a reversible one-electron oxidation at negative potential (−0.29 V and −0.27 V, respectively), followed by an irreversible oxidation at positive potential (+0.81 V and +0.74 V, respectively). The oxidation wave at positive potential is ligand-centred, while the process at negative potential is ascribed to the Fe^{III}/Fe^{II} redox couple. This relatively low iron(II) oxidation potential is attributed to the presence of two negatively charged deprotonated ligands, which stabilise the iron(III) oxidation state.[49] A further irreversible oxidative step is observed at +1.03 V for **13**, whose peak amplitude is smaller than the other two oxidation signals. This step is assigned to oxidation of an electrogenerated species, presumably originating from an EC process at +0.74 V.

The two tetrairon(II) grids **7** and **8** exhibit similar oxidative properties attributed to the Fe^{III}/Fe^{II} redox couples. For example, the $(Fe^{II}_{LS})_2(Fe^{II}_{SC})_2$ grid **8** displays two pairs of reversible, monoelectronic metal-centred oxidations at +0.10/+0.16 V and +0.93/+1.08 V, respectively. The pair at lower potential is assigned to the two Fe^{II}_{LS} centres, which are each surrounded by two negatively charged terdentate units. In contrast, the Fe^{II}_{SC} sites are coordinated by neutral hydrazone moieties and the oxidation potential is therefore shifted to more positive values. The above electrochemical assignment is confirmed by the cyclic voltammogram of the $(Fe^{II}_{LS})_2Zn^{II}_2$ grid **9**, which exhibits only one pair of overlapping monoelectronic iron-centred oxidations at +0.10/+0.15 V (Figure 9, top).

The Fe^{III}/Fe^{II} redox potential of iron imidazole complexes shifts negatively upon deprotonation, with $E_{1/2}$ decreasing by 235–345 mV per dissociated proton.[49] The 770 mV gap separating the second and third oxidation potentials in **8** reflects double deprotonation at the Fe^{II}_{LS} site, supplemented by a potential shift due to electronic communication between Fe^{II}_{SC} and two adjacent Fe^{III} centres. Interestingly, the electronic interaction between two *diagonally* opposed iron sites depends on the oxidation state of the remaining metallic centres. Thus, $\Delta E_{1/2}(2nd-1st) = 60$ mV, while $\Delta E_{1/2}(4th-3rd)$ is significantly larger at 150 mV. This behaviour is mimicked by the tetrairon(II) grid **7** and has previously been reported for a $[Fe^{II}_4L_4]^{8+}$ grid array based on a neutral bis(terdentate) scaffold.[2b]

The major influence on the iron(II) oxidation potential is the charge on the ligand binding pocket, rather than the Fe^{II} spin state in the grid. This can be seen by a comparison of the Fe^{III}/Fe^{II} redox couples in complexes **2**, **5**, **7**, **8** and **9**. Grids **2**, **5**, **7** and **8** exhibit similar redox potentials for Fe^{II} oxidation at the neutral binding site, regardless of iron(II) spin state. In contrast, only the grids **7**–**9** possessing Fe^{II} ions coordinated to a negatively charged site present a negative shift in the Fe^{II} oxidation potential.

Conclusion

A three-tiered synthetic route has been used to contruct an extended family of heterometallic $[2\times2]$ $[Co^{III}_2M^2_2(L^-)_4]^{6+}$ grid-type arrays ($M^2 = Co^{II}$, Fe^{II}, Zn^{II}). This approach encompasses regioselective, redox and enantioselective features and is based on the stepwise construction of bis(terdentate) hydrazone ligands. These ligands contain both ionisable and nonionisable compartments, thus allowing modification of the cobalt oxidation state according to the charge on the hydrazone moiety. The physical properties of the metalloarrays can be tuned by changing the type of 2-pyrimidine substituent.

The synthetic strategy can be adapted to prepare a series of $[(Fe^{II}_{LS})_2M^2_2(L^-)_4]^{4+}$ complexes incorporating two diagonally located low-spin Fe^{II} ions situated in negatively charged octahedral binding sites. The secondary metal ion M^2 was selected as Fe^{II} or Zn^{II} and is located at the neutral, *N*-methylated hydrazone site. The steric effect of the peripheral 6-pyridine substituent governs the iron(II) spin state at the neutral binding pocket. This allows an unusual mixed-spin-state grid to be assembled, which features two low-spin and two spin-crossover Fe^{II} centres across the grid diagonals.

The secondary metal ion M^2 and the pyrimidine/pyridine substituents strongly influence the magnetic properties of the grid. This was revealed by ^{1}H NMR spectroscopic studies conducted in [D$_3$]acetonitrile. As expected, the ^{1}H NMR spectra were diamagnetic for $M^2 = Zn^{II}$ or Fe^{II}_{LS} (M^1 = diamagnetic, low-spin Co^{III} or Fe^{II}), but paramagnetically shifted when paramagnetic ions Co^{II} or Fe^{II}_{HS} were present. Interestingly, the Fe^{II} ions can be low-spin, high-spin or spin-crossover centres depending on the central 2-pyrimidine (R) and external 6-pyridine (R′) groups. For example, the $[Co^{III}_2Fe^{II}_2(L^-)_4]^{6+}$ complex is diamagnetic when R = H (low-spin Fe^{II}), but paramagnetic when R = Ph (high-spin Fe^{II}).

Electrochemical studies were performed for all the heterometallic grid arrays and their respective mononuclear precursor complexes. The grids act as electron reservoirs and exhibit a series of monoelectronic reversible ligand-based reduction steps, which generally occur in pairs. The stability towards reduction crucially depends on the type of 2-pyrimidine substituent (R), with up to six reversible ligand-based reductions observed for grids **5** and **6** (R = Ph). Oxidation of the ligand is usually irreversible, although a notable exception is the reversible behaviour displayed by **4**.

Although all reduction steps below −1.0 V are formally centred on the ligand, it is clear that the metal ion modulates both the redox potential and the potential shift ($\Delta E_{1/2}$) separating each pair of reductions. This is readily seen by a comparison of $[Co^{III}_2M^2_2\mathbf{B}_4]^{6+}$ grids **4**–**6**, in which $\Delta E_{1/2}$ follows the M^2 sequence $Co^{II} > Fe^{II} > Zn^{II}$. A similar trend has been noted for homometallic $[M^{II}_4L_4]^{8+}$ grids based on homoditopic bis(hydrazone) ligands ($M^{II} = Co^{II}$, Fe^{II}, Zn^{II}).[2d]

Individual metal ions can be targeted electrochemically in the heterometallic grid motif. For example, grids **2** and **5** each incorporate two Co^{III} and two Fe^{II} centres that can be selectively reduced or oxidised, respectively. The metal-cen-

tred redox properties of mixed-valence grid **1** and tetra-iron(II) grids **7**,**8** are particularly intriguing. Both these examples show how the redox potential of the M^{III}/M^{II} couple can be controlled according to the charge on the ligand binding pocket. This feature allows selective electrochemical switching between $[M^{II}_2M^{II}_2]$, $[M^{III}_2M^{III}_2]$ and multiple mixed-valence electronic configurations.

In conclusion, heterometallic grids based on hydrazone ligands possess a range of desirable physicochemical and structural features, including: 1) two types of metal ion that can be introduced at specific sites in a [2×2] array; 2) magnetic properties that can be tuned according to the type of metal and ligand substituent; 3) local addressability through external stimuli, such as temperature or electrochemical potential; 4) thermally induced spin crossover and 5) electronic multistability, whereby the grid can exist in "on" or "off" states by manipulating the redox levels of the ligand and/or the metal. This type of metalloarray offers a wide palette of locally tunable features for supramolecular electronics. It thus represents a promising model for the development of future information storage devices incorporating multilevel redox and magnetic activity.

Experimental Section

General: Reagents were obtained from commercial suppliers and used without further purification unless otherwise noted. Chromatography was carried out on Merck silica gel 60 (0.063–0.200 mm) or Merck aluminium oxide 90 standardised. 4,6-Dichloropyrimidine, 97% (Aldrich) was purified by chromatography on silica gel (eluent: $CHCl_3$) prior to use. 4,6-Dichloro-2-phenylpyrimidine,[50] 4-chloro-6-hydrazinopyrimidine[14] and 4-chloro-6-hydrazino-2-phenylpyrimidine[15] were prepared according to literature procedures.

Electrochemistry: All compounds were studied in CH_2Cl_2 + 0.1 M Bu_4NPF_6 and in CH_3CN + 0.1 M Bu_4NPF_6, respectively. The electrochemical measurements were carried out at room temperature (20 °C) in CH_2Cl_2 containing 0.1 M Bu_4NPF_6 in a classical three-electrode cell. The electrochemical cell was connected to a computerised multipurpose electrochemical device (Autolab, Eco Chemie BV, The Netherlands) controlled by a GPES software (v. 4.7) running on a PC computer. The working electrode was a glassy carbon (GC) disk electrode (diameter: 3 mm) used either motionless for cyclic voltammetry (10 mV s^{-1} to 10 V s^{-1}) or as a rotating disk electrode. The auxiliary electrode was a platinum wire, and the reference electrode was an aqueous Ag/AgCl/KCl (sat.) electrode. All potentials are referred to the ferrocenium/ferrocene (Fc^+/Fc) couple used as the internal standard in agreement with the IUPAC recommendation.[51] Under our experimental conditions, ferrocene was oxidised at +0.40 V versus Ag/AgCl. The accessible potential domain ranged from +1.4 to −2.4 V versus Fc^+/Fc. CH_2Cl_2 (Merck, spectroscopic grade) was dried over molecular sieves (4 Å) and stored under argon. Bu_4NPF_6 (Fluka, electrochemical grade) was used as received. The electrolyte was degassed by bubbling argon through the solution for at least 5 min, and an argon flow was kept over the solution during measurements.

Studies carried out in CH_3CN were made in a glovebox under drastic exclusion of water and oxygen (less than 2 ppm). The classical three-electrode cell was connected to a Princeton Applied research potentiostat 263, controlled by a Powerlab/Echem electrochemical system (ADInstruments, USA). The working electrode was a platinum disk (2 mm in diameter), the auxiliary electrode a platinum wire, and the pseudo-reference electrode was also a platinum wire. Ferrocene, used as an internal standard, was introduced to the solution at the end of the study. All given potentials are therefore given versus ferrocene. CH_3CN (Merck, spectroscopic grade) and Bu_4NPF_6 (dried at 65 °C for 24 h) were introduced in the glove box. Bu_4NPF_6 was solubilised in CH_3CN inside the glove box and the solution was then percolated over activated alumina. The available potentials on a platinum working electrode ranged from −2.5 to +2.1 V/Fc.

Square-wave voltammetry was carried out at 75 Hz, by using a square-wave amplitude of 25 mV and a potential step of 2.5 mV. Cyclic voltammetry was carried out at scan rates ranging from 0.1 to 10 V s^{-1}. Evolution of the peak current and the peak potential with scan rate indicated that most electron transfers were reversible, as shown by a peak current ratio equal to unity and constant peak potentials for scan rates up to 1 V s^{-1}. Careful analysis of the peak characteristics and log-plot slopes of the waves obtained by rotating disk voltammetry allowed us to determine the individual redox potentials for overlapping electron transfers.[52]

The number of exchanged electrons for each step was determined by comparison of the wave amplitudes, observed by rotating disk voltammetry, of known concentrations of grids and ferrocene. In our experimental conditions, the first reduction step of the corner complexes involves one electron, whereas the first reduction of the grid arrays involves two electrons.

Spectroelectrochemical experiments were carried out as described elsewhere.[53]

Instrumentation: UV/Vis spectra were recorded for 6×10^{-6} M solutions in MeCN or CH_2Cl_2 by using a Varian Cary 3E UV/Vis spectrophotometer. ^1H and ^{13}C NMR spectra were recorded on a Bruker Avance 400 MHz spectrometer by using the residual solvent peak as reference. The notation system used to assign the ^1H NMR spectra is shown in Figure 10.

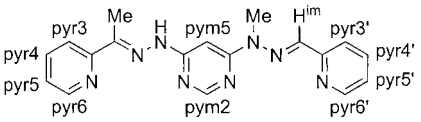

Figure 10. Ligand numbering system used to assign ^1H NMR spectra.

4-Hydrazino-6-(*N*-methylhydrazino)pyrimidine (16): *N*-Methylhydrazine (1.70 mL, 0.032 mol) was added to a suspension of 4-chloro-6-hydrazinopyrimidine (0.928 g, 6.42 mmol) in MeOH (15 mL) and the mixture heated to reflux under argon for 4 h. The volatiles were evaporated to afford a white solid, which was triturated with Et_2O and then suspended in ice cold MeOH (2 mL). The mixture was stirred for 0.5 h, filtered (to remove $MeNHNH_2$ contaminants) and washed carefully with cold MeOH. The product was obtained as a white solid, which was dried under vacuum (0.782 g, 79%). It was used in the subsequent step without further purification. ^1H NMR (400 MHz, [D$_6$]DMSO): δ = 7.90 (s, 1H; pym2), 7.58 (br s, 1H; NH), 6.27 (s, 1H; pym5), 4.40 (br s, 4H; NH_2), 3.18 ppm (s, 3H; Me); ^{13}C NMR (100 MHz, [D$_6$]DMSO): δ = 166.1, 165.1, 156.7, 80.3, 37.4 ppm; HR-FAB-MS: *m/z*: calcd for $C_5H_{11}N_6$: 155.1045; found: 155.1046 $[M+H]^+$.

4-Hydrazino-6-(*N*-methylhydrazino)-2-phenylpyrimidine (17): *N*-Methylhydrazine (2.76 mL, 0.052 mol) was added to a solution of 4-chloro-6-hydrazino-2-phenylpyrimidine (0.763 g, 3.46 mmol) in MeOH (15 mL) and the mixture heated to reflux under argon for 23 h. The volatiles were evaporated and the residue triturated with Et_2O. The crude white solid was dried under vacuum and used in the subsequent step without further purification. ^1H NMR (400 MHz, [D$_6$]DMSO): δ = 8.30 (m, 2H; *o*-Ph), 7.56 (s, 1H; NH), 7.42 (m, 3H; *m*-Ph, *p*-Ph), 6.28 (s, 1H; pym5), 4.60 (br s, 2H; NH_2), 4.19 (br s, 2H; NH_2), 3.32 ppm (s, 3H; Me); ^{13}C NMR (100 MHz, [D$_6$]DMSO): δ = 167.0, 165.8, 161.3, 139.3, 130.0, 128.3, 128.0, 79.3 ppm; HR-FAB-MS: *m/z* calcd for $C_{11}H_{15}N_6$: 231.1358; found: 231.1357 $[M+H]^+$.

Ligand 18: 2-Acetylpyridine (561 μL, 5.00 mmol) in MeOH (10 mL) was added dropwise over 15 mins to a solution of **16** (0.771 g, 5.00 mmol) in MeOH (20 mL) cooled in an ice bath. The mixture was stirred for 1.5 h

in the ice bath and then 18 h at room temperature. The precipitate was isolated by filtration, washed with MeOH and Et_2O, and then dried under vacuum to yield the product as a white solid (0.553 g, 43%). ^{1}H NMR (400 MHz, [D$_6$]DMSO): δ = 11.23 (br s, 1H; NH), 8.64 (m, 1H; pyr6), 8.40 (s, 2H; pyr3, pym2), 7.91 (m, 1H; pyr4), 7.45 (dd, J = 7.3 Hz, J' = 4.9 Hz, 1H; pyr5), 6.78 (br s, 1H; pym5), 5.34 (br s, 2H; NH_2), 3.41 (s, 3H; NMe), 2.49 ppm (s, 3H; CMe); ^{13}C NMR (100 MHz, [D$_6$]DMSO): δ = 154.5, 152.0, 151.8, 150.4, 150.3, 148.9, 137.3, 124.7, 121.4, 81.2, 13.1 ppm; HR-FAB-MS: m/z calcd for $C_{12}H_{16}N_7$: 258.1467; found: 258.1471 $[M+H]^+$; elemental analysis calcd (%) for $C_{12}H_{15}N_7 \cdot 2H_2O$: C 49.1, H 6.5, N 33.4; found: C 49.2, H 5.7, N 33.2.

Ligand 19: Synthesis as for ligand **18**, but with 2-acetylpyridine (197 μL, 1.76 mmol) in MeOH (5 mL), and **17** (0.405 g, 1.76 mmol) in MeOH (2 mL). The product was obtained as a white solid (0.255 g, 43%). ^{1}H NMR (400 MHz, [D$_6$]DMSO): δ = 10.68 (s, 1H; NH), 8.64 (d, J = 4.9 Hz, 1H; pyr6), 8.49 (d, J = 6.3 Hz, 2H; *o*-Ph), 8.26 (d, J = 8.3 Hz, 1H; pyr3), 7.93 (t, J = 7.8 Hz, 1H; pyr4), 7.57 (m, 3H; *m*-Ph, *p*-Ph), 7.45 (m, 1H; pyr5), 6.83 (s, 1H; pym5), 3.45 ppm (s, 3H; NMe); ^{13}C NMR (100 MHz, [D$_6$]DMSO): δ = 163.8, 154.8, 148.6, 137.8, 132.0, 128.9, 128.6, 124.4, 121.0, 81.5, 38.8, 12.8 ppm; HR-FAB-MS: m/z calcd for $C_{18}H_{20}N_7$: 334.1780; found: 334.1776 $[M+H]^+$; elemental analysis calcd (%) for $C_{18}H_{19}N_7 \cdot 2.5H_2O$: C 57.1, H 6.4, N 25.9; found: C 57.4, H 5.6, N 25.5.

Cobalt(III) complexes 10 and 20: Ligand **18** (88.7 mg, 0.345 mmol) and $Co(OAc)_2 \cdot 4H_2O$ (42.9 mg, 0.172 mmol) were heated at reflux in MeOH (5 mL) for 1 h to generate cobalt(III) complex **20** in situ. The solution was cooled and 2-pyridinecarboxaldehyde (65 μL, 0.689 mmol) added. The mixture was stirred at room temperature for 18 h and the solvent then evaporated under vacuum. The residue was purified by column chromatography on alumina, gradually increasing the polarity of the solvent system from CH_2Cl_2/MeCN (2:5) to MeCN to MeCN/MeOH (5:1). The solvent was removed from the red product band to afford the monoacetate salt [Co^{III}**A**$_2$]OAc as a brown solid (91.0 mg, 65%). ^{1}H NMR (400 MHz, [D$_4$]MeOD): δ = 8.59 (d, J = 3.9 Hz, 1H; pyr6′), 8.12 (d, J = 7.8 Hz, 1H; pyr3′), 8.03 (td, J = 7.8 Hz, J' = 1.3 Hz, 1H; pyr4), 7.95 (td, J = 7.6 Hz, J' = 1.7 Hz, 1H; pyr4′), 7.89 (s, 1H; H^{im}), 7.88 (d, J = 8.8 Hz, 1H; pyr3), 7.84 (d, J = 4.9 Hz, 1H; pyr6), 7.46 (s, 1H; pym2 or 5), 7.43 (ddd, J = 7.3 Hz, J' = 4.9 Hz, J'' = 1.0 Hz, 1H; pyr5′), 7.33 (m, 1H; pyr5), 7.14 (s, 1H; pym2 or 5), 3.55 (s, 3H; NMe), 3.15 ppm (s, 3H; CMe); ^{13}C NMR (100 MHz, [D$_4$]MeOD): δ = 171.0, 162.2, 160.4, 154.6, 153.7, 149.5, 148.8, 148.4, 140.9, 138.6, 137.2, 125.8, 123.8, 123.2, 120.4, 88.0, 28.7, 13.0 ppm; ES-MS: m/z: 750.8 [Co^{II}**A**(**A**+H)]$^+$.

Solubility problems in the self-assembly step hindered attempts to prepare grid **1** from $Co(BF_4)_2 \cdot 6H_2O$ and [Co^{III}**A**$_2$]OAc in MeCN. This difficulty was overcome by changing the [Co^{III}**A**$_2$]$^+$ counterion from acetate to hexafluorophosphate according to the procedure below:

[Co^{III}**A**$_2$]OAc was dissolved in the minimum amount of water and treated with a saturated aqueous solution of KPF_6. The precipitate was isolated by filtration and recrystallised from MeCN/Et_2O to afford the hexafluorophosphate salt [Co^{III}**A**$_2$]PF_6 (**10**) as a brown, crystalline solid (81.5 mg, 81% conversion from acetate salt). The ^{1}H NMR spectrum ([D$_4$]MeOD) and ES-MS: of **10** were identical to [Co^{III}**A**$_2$]OAc. The ^{1}H NMR spectrum of **10** was also recorded in [D$_3$]MeCN to allow direct comparison with the ^{1}H NMR spectra of grids **1**–**3** in [D$_3$]MeCN: ^{1}H NMR (400 MHz, [D$_3$]MeCN): δ = 8.60 (m, 1H; pyr6′), 8.10 (d, J = 8.3 Hz, 1H; pyr3′), 7.93 (td, J = 7.8 Hz, J' = 1.0 Hz, 1H; pyr4), 7.88 (s, 1H; H^{im}), 7.84 (td, J = 7.8 Hz, J' = 1.5 Hz, 1H; pyr4′), 7.71 (d, J = 5.9 Hz, 1H; pyr6), 7.71 (d, J = 7.8 Hz, 1H; pyr3), 7.39 (s, 1H; pym2 or 5), 7.35 (m, 1H; pyr5′), 7.22 (m, 1H; pyr5), 6.96 (s, 1H; pym2 or 5), 3.49 (s, 3H; NMe), 3.05 ppm (s, 3H; CMe); UV/Vis (MeCN): λ_{max} (ε) = 468 (6.9), 320 nm (7.0 × 10^4 dm^3 mol^{-1} cm^{-1}); elemental analysis calcd (%) for $CoC_{36}H_{34}N_{16}PF_6 \cdot 2H_2O$: C 46.5, H 4.1, N 24.1; found: C 46.3, H 4.0, N 23.9.

Cobalt(III) complexes 11 and 21: Ligand **19** (49.4 mg, 0.148 mmol) and $Co(OAc)_2 \cdot 4H_2O$ (18.5 mg, 0.074 mmol) were heated at reflux in H_2O/MeOH (7:3, 20 mL) for 2 h to generate cobalt(III) complex **11** in situ. The solution was cooled and 2-pyridinecarboxaldehyde (28 μL, 0.296 mmol) added. The mixture was stirred at room temperature for 15 h and the solvent then evaporated under vacuum. The sample was redissolved in the minimum amount of water and treated with a saturated aqueous solution of KPF_6. The precipitate was removed by filtration, washed with Et_2O and loaded onto an alumina column prepared in MeCN/CH_2Cl_2 (5:4). The eluent polarity was gradually increased from CH_2Cl_2 to MeCN/CH_2Cl_2 (1:2) to MeCN/CH_2Cl_2 (5:4). The solvent was evaporated from the orange product band to yield complex **11** as red-orange solid (33.0 mg, 42%). ^{1}H NMR (400 MHz, [D$_3$]MeCN): δ = 8.64 (m, 1H; pyr6′), 8.02 (d, J = 8.2 Hz, 1H; pyr3′), 7.91 (s, 1H; H^{im}), 7.86 (m, 2H; pyr4, pyr4′), 7.61 (tt, J = 7.4 Hz, J' = 1.2 Hz, 1H; *p*-Ph), 7.53 (br m, 1H; *m*-Ph), 7.50 (dd, J = 8.2 Hz, J = 0.9 Hz, 1H; pyr3), 7.41 (br m, 1H, *m*-Ph′), 7.38 (m, 2H; pyr5′, pyr6), 7.13 (m, 1H; pyr5), 6.90 (br d, 2H; *o*-Ph), 6.72 (s, 1H; pym5), 3.46 (s, 3H; NMe), 2.47 ppm (s, 3H; CMe); ^{13}C NMR (100 MHz, [D$_3$]MeCN): δ = 172.0, 168.5, 160.8, 160.7, 154.2, 149.8, 149.6, 147.3, 140.7, 140.1, 138.1, 136.7, 129.0, 127.9, 127.8, 127.5, 126.6, 125.3, 123.7, 122.0, 119.8, 87.2, 29.2, 13.6 ppm (slow rotation of the phenyl group at 298 K results in six separate ^{13}C signals for the phenyl carbon atoms); UV/Vis (MeCN): λ_{max} (ε) = 488 (6.6), 362 (sh, 3.1), 322 nm (8.1 × 10^4 dm^3 mol^{-1} cm^{-1}); ES-MS: m/z: 901.3 $[M-PF_6]^+$; elemental analysis calcd (%) for $CoC_{48}H_{42}N_{16}PF_6 \cdot 2H_2O$: C 53.2, H 4.3, N 20.7; found: C 53.3, H 4.1, N 20.2.

Iron(II) complex 12: Ligand **18** (0.190 g, 0.737 mmol) and $Fe(BF_4)_2 \cdot 6H_2O$ (0.124 g, 0.368 mmol) in MeOH (10 mL) were heated at reflux under argon for 1.5 h. The solution was cooled to room temperature and 2-pyridinecarboxaldehyde (0.140 mL, 1.47 mmol) added. The mixture was stirred at room temperature for 3.5 h and then concentrated to about 3 mL. The solution was added to Et_2O (30 mL) to give a red precipitate, which was isolated by filtration and subjected to chromatography on alumina (eluent: MeCN/CH_2Cl_2 1:1) to yield the product as a dark green solid (0.111 g, 40%). ^{1}H NMR (400 MHz, $CDCl_3$): δ = 8.55 (d, J = 4.1 Hz, 1H; pyr6′), 8.14 (d, J = 8.0 Hz, 1H; pyr3′), 7.75 (td, J = 7.7 Hz, J = 1.2 Hz, 1H; pyr4′), 7.69 (s, 1H; H^{im}), 7.43 (d, J = 5.3 Hz, 1H; pyr6), 7.35 (td, J = 7.6 Hz, J = 1.2 Hz, 1H; pyr4), 7.25 (d, J = 8.0 Hz, 1H; pyr3), 7.21 (m, 2H; pyr5′, pym2 or 5), 7.01 (s, 1H; pym2 or 5), 6.66 (t, J = 6.0 Hz, 1H; pyr5), 3.44 (s, 3H; NMe), 3.19 ppm (s, 3H; CMe); ^{13}C NMR (100 MHz, $CDCl_3$): δ = 162.6, 161.6, 157.5, 154.9, 152.2, 149.1, 136.5, 136.3, 134.6, 122.8, 121.5, 119.8, 118.6, 86.1, 29.4, 13.7 ppm; UV/Vis (MeCN): λ_{max} (ε) = 609 (0.97), 460 (sh, 4.4), 416 (8.3), 322 nm (5.3 × 10^4 dm^3 mol^{-1} cm^{-1}); ES-MS: m/z: 746.3 $[M]^+$, 374.1 $[M+2H]^{2+}$; elemental analysis calcd (%) for $FeC_{36}H_{34}N_{16} \cdot 2H_2O$: C 55.3, H 4.9, N 28.6; found: C 55.0, H 4.8, N 28.7.

Iron(II) complex 13: Ligand **18** (0.323 g, 1.26 mmol) and $Fe(BF_4)_2 \cdot 6H_2O$ (0.212 g, 0.628 mmol) in MeOH (20 mL) were heated at reflux under argon for 2 h. The solution was cooled to room temperature and 6-methyl-2-pyridinecarboxaldehyde (0.304 g, 2.51 mmol) added. The mixture was stirred at room temperature for 16 h and then concentrated to about 5 mL. The solution was added to Et_2O (30 mL) to give a red precipitate, which was isolated by filtration and subjected to chromatography on alumina (eluent: MeCN/CH_2Cl_2 1:2) to yield the product as a dark green solid (0.230 g, 47%). ^{1}H NMR (400 MHz, $CDCl_3$): δ = 7.96 (d, J = 7.8 Hz, 1H; pyr3′), 7.67 (s, 1H; H^{im}), 7.63 (t, J = 7.7 Hz, 1H; pyr4′), 7.42 (d, J = 5.4 Hz, 1H; pyr6), 7.34 (m, 1H; pyr4), 7.24 (d, J = 8.0 Hz, 1H; pyr3), 7.20 (s, 1H; pym2 or 5), 7.09 (d, J = 7.4 Hz, 1H; pyr5′), 6.99 (s, 1H; pym2 or 5), 6.45 (m, 1H; pyr5), 3.43 (s, 3H; NMe), 3.18 (s, 3H; CMe), 2.57 ppm (s, 3H; CMe′); ^{13}C NMR (100 MHz, $CDCl_3$): δ = 162.6, 161.6, 157.6, 157.4, 154.4, 152.1, 136.7, 136.5, 134.5, 122.3, 121.3, 118.4, 116.8, 86.0, 29.4, 24.3, 13.6 ppm; UV/Vis (MeCN): λ_{max} (ε) = 609 (0.37), 460 (sh, 4.0), 419 (7.7), 325 nm (4.1 × 10^4 dm^3 mol^{-1} cm^{-1}); ES-MS: m/z: 774.3 $[M]^+$; elemental analysis calcd (%) for $FeC_{38}H_{38}N_{16} \cdot 1.5H_2O$: C 56.9, H 5.2, N 28.0; found: C 57.0, H 5.1, N 27.5.

Grid complex [Co$^{III}_2$Co$^{II}_2$A$_4$](PF$_6$)$_2$(BF$_4$)$_4$ (1): Complex **10** (33.7 mg, 37.6 mo μl) and $Co(BF_4)_2 \cdot 6H_2O$ (12.8 mg, 37.6 mo μl) were stirred in MeCN (2.5 mL) at room temperature for 18 h. The product was obtained as a dark red solid by recrystallisation from MeCN/Et_2O (33.3 mg, 75%). ^{1}H NMR (400 MHz, [D$_3$]MeCN): δ = 213.7, 158.1, 138.5 (pyr6, pym2 and H^{im}), 75.7 (pyr3′ or 5′), 73.3 (pym5), 54.3 (pyr3′ or 5′), 18.2 (pyr4′), 14.3 (CMe), 12.7 (pyr3), 11.4 (pyr6), 10.7 (pyr4), 7.9 (pyr5), 6.9 ppm (NMe); UV/Vis (MeCN): λ_{max} (ε) = 462 (12.3), 364 (5.8), 325 (6.2), 277 nm (7.4 × 10^4 dm^3 mol^{-1} cm^{-1}); ES-MS: m/z: 1040.2 $[M-2BF_4]^{2+}$, 1011.2 $[M-PF_6-BF_4]^{2+}$, 982.1 $[M-2PF_6]^{2+}$, 749.2 [Co^{III}**A**$_2$]$^+$, 672.2 [Co^{II}**A**(**A**+H)−C$_5$H$_4$N]$^+$, 664.4 $[M-3BF_4]^{3+}$, 645.1 $[M-PF_6-2BF_4]^{3+}$, 625.8

$[M-2PF_6-BF_4]^{3+}$, 476.6 $[M-4BF_4]^{4+}$, 462.1 $[M-PF_6-3BF_4]^{4+}$, 447.6 $[M-2PF_6-2BF_4]^{4+}$, 352.3 $[M-PF_6-4BF_4]^{5+}$, 340.7 $[M-2PF_6-3BF_4]^{5+}$, 269.4 $[M-2PF_6-4BF_4]^{6+}$; elemental analysis calcd (%) for $Co_4C_{72}H_{68}N_{32}P_2B_4F_{28}\cdot 6H_2O$: C 36.6, H 3.4, N 19.0; found: C 36.6, H 3.2, N 18.7.

Grid complex $[Co^{III}_2Fe^{II}_2A_4](PF_6)_2(BF_4)_4$ (2): Complex **10** (8.8 mg, 9.8 moμl) and $Fe(BF_4)_2\cdot 6H_2O$ (3.3 mg, 9.8 moμl) were heated at reflux in MeCN (7 mL) under argon for 24 h. The product was obtained as a brown solid by recrystallisation from MeCN/Et_2O (7.5 mg, 68%). ^{1}H NMR (400 MHz, [D$_3$]MeCN): $\delta=9.63$ (s, 1H; H^{im}), 7.95 (d, $J=7.8$ Hz, 1H; pyr3′), 7.89 (t, $J=7.6$ Hz, 1H; pyr4), 7.76 (d, $J=7.3$ Hz, 1H; pyr3), 7.71 (t, $J=7.3$ Hz, 1H; pyr4′), 7.56 (d, $J=5.4$ Hz, 1H; pyr6), 7.46 (d, $J=4.9$ Hz, 1H; pyr6′), 7.22 (t, $J=6.1$ Hz, 1H; pyr5), 7.00 (t, $J=6.1$ Hz, 1H; pyr5′), 6.50 (s, 1H; pym5), 5.55 (s, 1H; pym2), 4.44 (s, 3H; NMe), 3.25 ppm (s, 3H; CMe); ^{13}C NMR (100 MHz, [D$_3$]MeCN): $\delta=$ 168.4, 159.0, 158.4, 158.0, 154.2, 153.4, 151.2, 145.2, 141.7, 138.6, 128.6, 126.8, 126.6, 125.8, 84.8, 35.0, 14.8 ppm; UV/Vis (MeCN): λ_{max} (ε) = 607 (0.96), 458 (12.4), 349 (9.0), 276 nm (7.1×10^4 dm^{3}mol^{-1}cm^{-1}); ES-MS: *m/z*: 979.2 $[M-2PF_6]^{2+}$, 749.3 $[Co^{III}\mathbf{A}_2]^+$, 623.8 $[M-2PF_6-BF_4]^{3+}$, 446.1 $[M-2PF_6-2BF_4]^{4+}$, 412.1 $[Co^{III}Fe^{II}\mathbf{A}_2F]^{2+}$, 339.5 $[M-2PF_6-3BF_4]^{5+}$, 268.4 $[M-2PF_6-4BF_4]^{6+}$; elemental analysis calcd (%) for $Fe_2Co_2C_{72}H_{68}N_{32}P_2B_4F_{28}\cdot 8H_2O$: C 36.2, H 3.5, N 18.7; found: C 36.6, H 3.3, N 18.4.

Grid complex $[Co^{III}_2Zn^{II}_2A_4](PF_6)_2(BF_4)_4$ (3): Synthesis as for grid complex **1**, using complex **10** (40.0 mg, 44.7 moμl) and $Zn(BF_4)_2\cdot x H_2O$ (x ~6–7) (16.3 mg); brown solid (35.9 mg, 71%). ^{1}H NMR (400 MHz, [D$_3$]MeCN): $\delta=8.53$ (s, 1H; H^{im}), 8.14 (td, $J=7.8$ Hz, $J'=1.5$ Hz, 1H; pyr4′), 7.98 (d, $J=7.8$ Hz, 1H; pyr3′), 7.95 (td, $J=7.8$ Hz, $J'=1.5$ Hz, 1H; pyr4), 7.88 (dd, $J=4.4$ Hz, $J'=1.0$ Hz, 1H; pyr6′), 7.69 (dd, $J=7.8$ Hz, $J'=1.0$ Hz, 1H; pyr3), 7.61 (dd, $J=5.8$ Hz, $J'=1.0$ Hz, 1H; pyr6), 7.35 (ddd, $J=7.6$ Hz, $J'=5.3$ Hz, $J''=1.1$ Hz; pyr5′), 7.29 (m, 1H; pyr5), 6.53 (s, 1H; pym5), 6.22 (d, $J=1.0$ Hz, 1H; pym2), 3.93 (s, 3H; NMe), 3.03 ppm (s, 3H; CMe); ^{13}C NMR (100 MHz, [D$_3$]MeCN): $\delta=$169.0, 158.8, 157.3, 154.8, 153.7, 150.9, 149.1, 146.4, 142.1, 141.6, 136.0, 128.3, 127.7, 129.0, 125.8, 86.0, 33.1, 14.6 ppm; UV/Vis (MeCN): λ_{max} (ε) = 462 (11.4), 439 (11.6), 362 (5.8), 346 (sh, 5.6), 276 nm (6.4×10^4 dm^{3}mol^{-1}cm^{-1}); ES-MS: *m/z*: 1047.1 $[M-2BF_4]^{2+}$, 1018.2 $[M-PF_6-BF_4]^{2+}$, 988.2 $[M-2PF_6]^{2+}$, 749.2 $[Co^{III}\mathbf{A}_2]^+$, 672.2 $[Co^{II}\mathbf{A}(\mathbf{A}+H)-C_5H_4N]^+$, 669.1 $[M-3BF_4]^{3+}$, 649.8 $[M-PF_6-2BF_4]^{3+}$, 630.5 $[M-2PF_6-BF_4]^{3+}$, 480.1 $[M-4BF_4]^{4+}$, 465.6 $[M-PF_6-3BF_4]^{4+}$, 451.1 $[M-2PF_6-2BF_4]^{4+}$, 416.1 $[Co^{III}Zn^{II}\mathbf{A}_2F]^{2+}$, 355.1 $[M-PF_6-4BF_4]^{5+}$, 343.5 $[M-2PF_6-3BF_4]^{5+}$, 271.7 $[M-2PF_6-4BF_4]^{6+}$; elemental analysis calcd (%) for $Zn_2Co_2C_{72}H_{68}N_{32}P_2B_4F_{28}\cdot 8H_2O$: C 35.9, H 3.5, N 18.6; found: C 36.2, H 3.2, N 18.3.

Grid complex $[Co^{III}_2Co^{II}_2B_4](PF_6)_2(BF_4)_4$ (4): Complex **11** (22.5 mg, 21.5 moμl) and $Co(BF_4)_2\cdot 6H_2O$ (7.3 mg, 21.5 moμl) were stirred in MeCN (2 mL) at room temperature for 18 h. The product was obtained as a dark red solid by recrystallisation from MeCN/Et_2O (18.5 mg, 67%). ^{1}H NMR (400 MHz, [D$_3$]MeCN): $\delta=$216.4, 195.0 (pyr6 and H^{im}), 81.6 (pym5), 64.6 (pyr3′ or 5′), 47.2 (pyr3′ or 5′), 23.3 (NMe), 13.8 (pyr6), 12.7 (pyr5), 10.5 (pyr4), 7.9 (pyr3), 1.6 (CMe), 1.4 (pyr4′), −0.8 (*p*-Ph), −4.3 (*m*-Ph), −4.7 (*o*-Ph), −6.4 (*m*-Ph′), −33.5 ppm (*o*-Ph′); UV/Vis (MeCN): λ_{max} (ε) = 483 (12.8), 458 (12.7), 367 (5.5), 347 (6.0), 275 nm (7.7×10^4 dm^{3}mol^{-1}cm^{-1}); ES-MS: *m/z*: 1192.2 $[M-2BF_4]^{2+}$, 1163.2 $[M-PF_6-BF_4]^{2+}$, 1134.3 $[M-2PF_6]^{2+}$, 766.2 $[M-3BF_4]^{3+}$, 746.5 $[M-PF_6-2\ BF_4]^{3+}$, 727.2 $[M-2PF_6-BF_4]^{3+}$, 552.9 $[M-4BF_4]^{4+}$, 538.4 $[M-PF_6-3BF_4]^{4+}$, 523.6 $[M-2PF_6-2\ BF_4]^{4+}$, 413.3 $[M-PF_6-4BF_4]^{5+}$, 401.7 $[M-2PF_6-3BF_4]^{5+}$, 320.3 $[M-2PF_6-4BF_4]^{6+}$; elemental analysis calcd (%) for $Co_4C_{96}H_{84}N_{32}P_2B_4F_{28}\cdot 6H_2O$: C 43.2, H 3.6, N 16.8; found: C 43.4, H 3.5, N 16.4.

Grid complex $[Co^{III}_2Fe^{II}_2B_4](PF_6)_2(BF_4)_4$ (5): Complex **11** (41.2 mg, 39.4 moμl) and $Fe(BF_4)_2\cdot 6H_2O$ (13.3 mg, 39.4 moμl) were heated at reflux in MeCN (10 mL) under argon for 26 h. The product was obtained as a dark red-brown solid by recrystallisation from MeCN/Et_2O (37.6 mg, 75%). ^{1}H NMR (400 MHz, [D$_3$]MeCN): $\delta=$219.5, 150.4, 87.0, 56.2, 33.9, 21.2, 18.8, 10.2, 8.2, 8.0, 7.4, 2.7, 2.5, −4.2, −11.2, −13.5, −36.1 ppm (a full ^{1}H NMR spectroscopic assignment was not possible for **5** because of the fast T_1 relaxation times, which were generally considerably shorter than the corresponding T_1 values for grid **4**); UV/Vis (MeCN): λ_{max} (ε) = 485 (14.0), 461 (14.5), 369 (5.5), 350 (5.9), 274 nm (8.2×10^4 dm^{3}mol^{-1}cm^{-1}); ES-MS: *m/z*: 1189.2 $[M-2BF_4]^{2+}$, 1160.3 $[M-PF_6-BF_4]^{2+}$, 1131.3 $[M-2PF_6]^{2+}$, 763.8 $[M-3BF_4]^{3+}$, 744.5 $[M-PF_6-2BF_4]^{3+}$, 725.2 $[M-2PF_6-BF_4]^{3+}$, 551.4 $[M-4BF_4]^{4+}$, 536.9 M $-PF_6-3BF_4]^{4+}$, 522.1 $[M-2PF_6-2BF_4]^{4+}$, 412.1 $[M-PF_6-4BF_4]^{5+}$, 400.5 $[M-2PF_6-3BF_4]^{5+}$, 319.3 $[M-2PF_6-4BF_4]^{6+}$; elemental analysis calcd (%) for $Co_2Fe_2C_{96}H_{84}N_{32}P_2B_4F_{28}\cdot 6H_2O$: C 43.3, H 3.6, N 16.9; found: C 43.7, H 3.7, N 16.9.

Grid complex $[Co^{III}_2Zn^{II}_2B_4](PF_6)_2(BF_4)_4$ (6): Synthesis as for grid complex **4**, from complex **11** (26.4 mg, 25.2 moμl) and $Zn(BF_4)_2\cdot x H_2O$ (x ~6–7) (9.2 mg); dark red solid (23.5 mg, 73%). ^{1}H NMR (400 MHz, [D$_3$]MeCN): $\delta=7.99$ (t, $J=7.6$ Hz, 1H; *p*-Ph), 7.89 (td, $J=7.8$ Hz, $J'=1.5$ Hz, 1H; pyr4′), 7.86 (t, $J=7.6$ Hz, 1H; *m*-Ph), 7.82 (td, $J=7.7$ Hz, $J'=1.3$ Hz, 1H; pyr4), 7.72 (s, 1H; H^{im}), 7.58 (d, $J=7.8$ Hz, 1H; pyr3′), 7.47 (dd, $J=7.8$ Hz, $J'=1.5$ Hz, 1H; pyr3), 7.42 (d, $J=4.4$ Hz, 1H; pyr6′), 7.35 (t, $J=7.6$ Hz, 1H; *m*-Ph′), 7.21 (m, 1H; pyr5), 7.16 (ddd, $J=7.6$ Hz, $J'=5.1$ Hz, $J''=1.0$ Hz, 1H; pyr5′), 7.05 (dd, $J=5.9$ Hz, $J'=1.0$ Hz, 1H; pyr6), 6.62 (d, $J=7.3$ Hz, 1H; *o*-Ph), 6.22 (s, 1H; pym5), 5.66 (d, $J=7.3$ Hz, 1H; *o*-Ph′), 3.49 (s, 3H; NMe), 2.56 ppm (s, 3H; CMe); ^{13}C NMR (100 MHz, [D$_3$]MeCN): $\delta=$168.9, 168.8, 159.1, 156.9, 154.2, 150.9, 148.0, 145.0, 141.3, 141.2, 135.0, 134.4, 131.7, 129.6, 129.2, 128.4, 127.6, 126.9, 126.6, 125.1, 124.0, 86.8, 32.9, 14.8 ppm; UV/Vis (MeCN): λ_{max} (ε) = 482 (15.1), 457 (15.1), 363 (6.9), 349 (7.3), 269 nm (8.7×10^4 dm^{3}mol^{-1}cm^{-1}); ES-MS: *m/z*: 1199.2 $[M-2BF_4]^{2+}$, 1169.7 $[M-PF_6-BF_4]^{2+}$, 1140.3 $[M-2PF_6]^{2+}$, 770.5 $[M-3BF_4]^{3+}$, 751.2 $[M-PF_6-2BF_4]^{3+}$, 731.5 $[M-2PF_6-BF_4]^{3+}$, 556.1 $[M-4BF_4]^{4+}$, 541.6 $[M-PF_6-3BF_4]^{4+}$, 527.1 $[M-2PF_6-2BF_4]^{4+}$, 415.9 $[M-PF_6-4BF_4]^{5+}$, 404.3 $[M-2PF_6-3BF_4]^{5+}$; elemental analysis calcd (%) for $Co_2Zn_2C_{96}H_{84}N_{32}P_2B_4F_{28}\cdot 6H_2O$: C 43.0, H 3.6, N 16.7; found: C 43.2, H 3.5, N 16.5.

Grid complex $[(Fe^{II}_{LS})_2(Fe^{II}_{LS})_2A_4](BF_4)_4$ (7): Complex **12** (11.2 mg, 15.0 moμl) and $Fe(BF_4)_2\cdot 6H_2O$ (5.1 mg, 15.0 moμl) were heated at reflux in MeCN (12 mL) under argon for 5 d. The product was obtained as a dark brown solid by layering a concentrated MeCN solution (2 mL) with Et_2O (9.1 mg, 62%). ^{1}H NMR (400 MHz, [D$_3$]MeCN): $\delta=9.38$ (s, 1H; H^{im}), 7.79 (d, $J=8.3$ Hz, 1H; pyr3′), 7.60 (t, $J=7.8$ Hz, 1H; pyr4′), 7.44 (m, 2H; pyr3, pyr4), 7.34 (d, $J=4.9$ Hz, 1H; pyr6′), 7.20 (d, $J=4.9$ Hz, 1H; pyr6), 6.89 (t, $J=6.4$ Hz, 1H; pyr5′), 6.71 (t, $J=6.1$ Hz, 1H; pyr5), 6.10 (s, 1H; pym5), 5.30 (s, 1H; pym2), 4.35 (s, 3H; NMe), 3.28 ppm (s, 3H, CMe); ^{13}C NMR (100 MHz, [D$_3$]MeCN): $\delta=$168.6, 161.0, 158.6, 158.0, 155.7, 154.2, 152.6, 151.9, 141.2, 137.8, 136.5, 125.4, 124.2, 121.5, 82.5, 34.4, 13.6 ppm; UV/Vis (MeCN): λ_{max} (ε) = 611 (0.65), 460 (6.5, *sh.*), 395 (12.1), 330 (5.0), 273 nm (4.4×10^4 dm^{3}mol^{-1}cm^{-1}); ES-MS: *m/z*: 401.1 $[M-4BF_4]^{4+}$; elemental analysis calcd (%) for $Fe_4C_{72}H_{68}N_{32}B_4F_{16}\cdot 8H_2O$: C 41.3, H 4.0, N 21.4; found: C 41.1, H 3.9, N 21.6.

Grid complex $[(Fe^{II}_{LS})_2(Fe^{II}_{SC})_2C_4](BF_4)_4$ (8): Complex **13** (60.0 mg, 77.5 moμl) and $Fe(BF_4)_2\cdot 6H_2O$ (26.1 mg, 77.5 moμl) were heated at reflux in MeCN (10 mL) under argon for 21 h. The product was obtained as a dark brown solid by recrystallisation from MeCN/Et_2O (65.0 mg, 84%). ^{1}H NMR (400 MHz, [D$_3$]MeCN, 298 K): $\delta=48.0$ (s, 1H), 25.6 (s, 1H), 17.0 (s, 1H), 15.3 (m, 2H), 7.7 (s, 1H), 7.1 (t, $J=7.1$ Hz, 1H; pyr4), 6.9 (d, $J=4.8$ Hz, 1H; pyr6), 6.6 (s, 3H), 5.9 (d, $J=9.5$ Hz, 1H; pyr3), 5.7 (m, 1H; pyr5), 5.6 (s, 3H), 4.2 ppm (s, 3H); UV/Vis (MeCN): λ_{max} (ε) = 610 (0.60), 460 (sh, 7.0), 407 (11.5), 274 nm (12.1×10^4 dm^{3}mol^{-1}cm^{-1}); ES-MS: *m/z*: 582.5 $[M-3BF_4]^{3+}$, 415.4 $[M-4BF_4]^{4+}$; elemental analysis calcd (%) for $Fe_4C_{76}H_{76}N_{32}B_4F_{16}\cdot 8H_2O$: C 42.4, H 4.3, N 20.8; found: C 42.2, H 4.1, N 20.6.

Grid complex $[(Fe^{II}_{LS})_2Zn^{II}_2C_4](BF_4)_4$ (9): Complex **13** (50.0 mg, 64.5 moμl) and $Zn(BF_4)_2\cdot x H_2O$ (*x* ~6–7) (23.6 mg) in MeCN (10 mL) under argon were stirred at room temperature for 17 h and then heated at reflux for 26 h. The mixture was filtered and purified by recrystallisation from MeCN/Et_2O to yield a black solid (59.2 mg, 90%). ^{1}H NMR (400 MHz, [D$_3$]MeCN): $\delta=8.27$ (s, 1H; H^{im}), 7.91 (t, $J=7.6$ Hz, 1H; pyr4′), 7.71 (d, $J=7.3$ Hz, 1H; pyr3′), 7.47 (m, 2H; pyr3, pyr4), 7.31 (d, $J=5.4$ Hz, 1H; pyr6), 7.18 (d, $J=7.3$ Hz, 1H; pyr5′), 6.79 (m, 1H; pyr5), 6.12 (s, 1H; pym5), 5.84 (s, 1H; pym2), 3.97 (s, 3H; NMe), 3.20 (s, 3H; CMe), 2.17 ppm (s, 3H; CMe′); ^{13}C NMR (100 MHz, [D$_3$]MeCN): $\delta=$ 169.0, 161.1, 160.2, 154.5, 153.6, 153.4, 152.0, 146.5, 141.3, 136.4, 131.7,

127.8, 124.1, 121.5, 82.3, 32.6, 22.4, 13.7 ppm; UV/Vis (MeCN): λ_{max} (ε) = 608 (0.61), 455 (sh, 8.0), 407 (15.3), 344 (6.0), 273 nm (5.9×10^4 dm^{3}mol^{-1}cm^{-1}); ES-MS: *m/z*: 420.1 $[M-4BF_4]^{4+}$; elemental analysis calcd (%) for $Fe_2Zn_2C_{76}H_{76}N_{32}B_4F_{16}\cdot6H_2O$: C 42.8, H 4.2, N 21.0; found: C 42.5, H 4.3, N 21.4.

Single-crystal X-ray analyses

Corner complex $[Co^{III}A_2]PF_6$ (10): Single crystals of complex **10** were obtained from vapour diffusion of Et_2O into MeCN. Measurements at 173.0(1) K by Enraf Nonius Kappa CCD diffractometer, $Mo_{K\alpha}$ radiation, $\lambda = 0.71073$ Å. The data were processed with Denzo-SMN v0.93.0.[54] The structure was solved in acentric tetragonal space group $I\bar{4}2d$ (no. 122) by using direct methods with SHELXS.[55] Refinement on F^2 with SHELXL-97.[56] These procedures were run under Wingx program[57] suite. The hydrogen atoms of the complex were calculated to their idealised positions with isotropic temperature factors and refined as riding atoms. The very heavily disordered solvent acetonitrile and water molecules could not be properly located and the residual electron density was modelled as carbon, nitrogen and oxygen atoms without any attempt to build chemically reasonable solvent molecules. No attempts were made to localise hydrogen atoms on the disordered parts of the structure.

Grid complex $[Co^{III}_2Zn^{II}_2B_4](PF_6)_3(BF_4)_3$ (6): Single crystals of grid complex **6** were obtained by liquid diffusion of Et_2O into MeCN. The crystal data were collected at 173 K on a Kappa CCD diffractometer using monochromated $Mo_K\alpha$ radiation ($\lambda = 0.71073$ Å). The structures were solved by direct methods. Hydrogen atoms were introduced as fixed contributors at calculated positions (C–H = 0.95 Å, B(H) = 1.3 Bequiv). Final difference maps revealed no significant maxima. All calculations were done using the Nonius OpenMoleN package.[58] Neutral atom scattering factor coefficients and anomalous dispersion coefficients were taken from a standard source.[59]

Grid complex $[Fe^{II}_2Zn^{II}_2C_4](BF_4)_4$ (9): The crystals were obtained by vapour diffusion of Et_2O into $MeNO_2$. The single-crystal X-ray diffraction was performed using a Nonius KappaCCD diffractometer with graphite monochromatised $Mo_{K\alpha}$ ($\lambda = 0.71073$ Å) radiation. Collect software was used for the measurement and DENZO-SMN[54] for the processing of the data. The structure was solved and refined by full-matrix least-squares on F^2 using the WinGX-software package[57] which utilises the SHELXS-97[60] and SHELXL-97[56] modules. Hydrogen atoms were refined using a riding model. Neither the second BF_4 anion nor the disordered solvent molecules of the asymmetric unit could be localised. The disordered solvent treatment SQUEEZE/BYPASS[61] was applied to the structure.

Details of the data collection and refinement for complexes **6**, **9** and **10** are given in Table 3.

Table 3. X-ray crystallographic data for complexes **6**, **9** and **10**.

	6	**9**	**10**
formula	$Co_2Zn_2C_{110}H_{113}N_{39}B_3F_{30}O_4P_3$	$Zn_2Fe_2C_{76}H_{76}N_{32}B_2F_{28}$	$Co_2C_{81.25}H_{71}N_{33.75}F_{12}O_{0.50}P_2$
M_r	2989.30	1847.70	1936.02
T [K]	173	173	173
crystal system	monoclinic	monoclinic	tetragonal
space group	$P12_1/n1$	$C2/c$	$I\bar{4}2d$
a [Å]	17.7075(1)	24.2080(11)	19.8810(6)
b [Å]	23.2663(2)	22.5149(12)	19.8850(7)
c [Å]	32.9010(3)	23.3468(11)	48.0540(16)
β [°]	93.685(5)	93.055(3)	90
V [Å^3]	13526.8(2)	12706.9(11)	18997.4(11)
Z	4	4	8
μ [mm^{-1}]	0.732	0.651	0.468
ρ [g cm^{-3}]	1.47	0.969	1.354
$\Delta\rho$(max/min) [e Å^{-3}]	1.120/−0.919	0.393/−0.347	0.423/−0.385
reflns collected/unique	39246/20528	33643/10816	35257/7836
cell refinement	–	9924	5944
parameters	1744	555	594
R_1 [$I > n\sigma(I)$]	0.098 [$I > 3\sigma(I)$]	0.0651 [$I > 2\sigma(I)$]	0.0851 [$I > 2\sigma(I)$]
wR_2 [$I > n\sigma(I)$]	0.133 [$I > 3\sigma(I)$]	0.1745 [$I > 2\sigma(I)$]	0.2150 [$I > 2\sigma(I)$]

CCDC-256044 (complex **10**), CCDC-256045 (grid **6**) and CCDC-256886 (grid **9**) contain the supplementary crystallographic data for this paper. These data can be obtained free of charge from the Cambridge Crystallographic Data Centre via www.ccdc.cam.ac.uk/data_request/cif.

Acknowledgements

This work was supported by a CNRS postdoctoral fellowship (L.H.U.). We thank R. Graff, J.-P. Kintzinger and P. Maltese for performing the two-dimensional NMR experiments.

[1] J.-M. Lehn, *Supramolecular Chemistry: Concepts and Perspectives*, VCH, Weinheim, **1995**; D. N. Hendrickson, D. M. Adams, C.-C. Wu, S. M. J. Aubin in *Magnetism: A Supramolecular Function* (Ed.: O Kahn), Kluwer Academic, Dordrecht (The Netherlands), **1996**, p. 357; M. Cavallini, F. Biscarini, S. Léon, F. Zerbetto, G. Bottari, D. A. Leigh, *Science* **2003**, *299*, 531.

[2] a) M. Ruben, E. Breuning, M. Barboiu, J.-P. Gisselbrecht, J.-M. Lehn, *Chem. Eur. J.* **2003**, *9*, 291; b) D. M. Bassani, J.-M. Lehn, S. Serroni, F. Puntoriero, S. Campagna, *Chem. Eur. J.* **2003**, *9*, 5936; c) D. M. Bassani, J.-M. Lehn, K. Fromm, D. Fenske, *Angew. Chem.* **1998**, *110*, 2534; *Angew. Chem. Int. Ed.* **1998**, *37*, 2364; d) L. H. Uppadine, J.-P. Gisselbrecht, J.-M. Lehn, *Chem. Commun.* **2004**, 718; e) L. Zhao, Z. Xu, H. Grove, V. A. Milway, L. N. Dawe, T. S. M. Abedin, L. K. Thompson, T. L. Kelly, R. G. Harvey, D. O. Miller, L. Weeks, J. G. Shapter, K. J. Pope, *Inorg. Chem.* **2004**, *43*, 3812; f) W. Kaim, B. Schwederski, A. Dogan, J. Fiedler, C. J. Kuehl, P. J. Stang, *Inorg. Chem.* **2002**, *41*, 4025.

[3] a) E. Breuning, M. Ruben, J.-M. Lehn, F. Renz, Y. Garcia, V. Ksenofontov, P. Gütlich, E. Wegelius, K. Rissanen, *Angew. Chem.* **2000**, *112*, 2563; *Angew. Chem. Int. Ed.* **2000**, *39*, 2504; b) M. Ruben, E. Breuning, J.-M. Lehn, V. Ksenofontov, F. Renz, P. Gütlich, G. B. M. Vaughan, *Chem. Eur. J.* **2003**, *9*, 4422; c) O. Kahn, C. J. Martinez, *Science* **1998**, *279*, 44; d) T. Glaser, *Angew. Chem.* **2003**, *115*, 5846; *Angew. Chem. Int. Ed.* **2003**, *42*, 5668; e) A. Boussekson, G. Molnár, P. Demont, J. Menegotto, *J. Mater. Chem.* **2003**, *13*, 2069; f) O. Kahn, J. Kröber, C. Jay, *Adv. Mater.* **1992**, *4*, 718; g) Y. Sunatsuki, Y. Ikuta, N. Matsumoto, H. Ohta, M. Kojima, S. Iijima, S. Hayami, Y. Maeda, S. Kaizaki, F. Dahan, J.-P. Tuchagues, *Angew. Chem.* **2003**, *115*, 1652; *Angew. Chem. Int. Ed.* **2003**, *42*, 1614.

[4] a) M. Ruben, J.-M. Lehn, G. Vaughan, *Chem. Commun.* **2003**, 1338; b) G. Ambrosi, P. Dapporton, M. Formica, V. Fusi, L. Giorgi, A. Guerri, M. Micheloni, P. Paoli, R. Pontellini, P. Rossi, *Chem. Eur. J.* **2003**, *9*, 800.

[5] M. Ruben, J. Rojo, F. J. Romero-Salguero, L. H. Uppadine, J.-M. Lehn, *Angew. Chem.* **2004**, *116*, 3728; *Angew. Chem. Int. Ed.* **2004**, *43*, 3644.

[6] a) O. Waldmann, J. Hassmann, P. Müller, G. S. Hanan, D. Volkmer, U. S. Schubert, J.-M. Lehn, *Phys. Rev. Lett.* **1997**, *78*, 3390; b) K. L. V. Mann, E. Psillakis, J. C. Jeffery, L. H. Rees, N. M. Harden, J. A. McCleverty, M. D. Ward, D. Gatteschi, F. Totti, F. E. Mabbs, E. J. L. McInnes, P. C. Riedi, G. M. Smith, *J. Chem. Soc. Dalton Trans.* **1999**, 339; c) L. K. Thompson, L. Zhao, Z. Xu, D. O. Miller, W. M. Reiff, *Inorg. Chem.* **2003**, *42*, 128.

[7] L. Zhao, Z. Xu, L. K. Thompson, S. L. Heath, D. O. Miller, M. Ohba, *Angew. Chem.* **2000**, *112*, 3244; *Angew. Chem. Int. Ed.* **2000**, *39*, 3114.
[8] A. Semenov, J. P. Spatz, M. Möller, J.-M. Lehn, B. Sell, D. Schubert, C. H. Weidl, U. S. Schubert, *Angew. Chem.* **1999**, *111*, 2701; *Angew. Chem. Int. Ed.* **1999**, *38*, 2547.
[9] J.-M. Lehn, *Science* **2002**, *295*, 2400; S. Leininger, B. Olenyuk, P. J. Stang, *Chem. Rev.* **2000**, *100*, 853; B. J. Holliday, C. A. Mirkin, *Angew. Chem.* **2001**, *113*, 2076; *Angew. Chem. Int. Ed.* **2001**, *40*, 2022; D. L. Caulder, K. N. Raymond, *J. Chem. Soc. Dalton Trans.* **1989**, 1185; C. J. Jones, *Chem. Soc. Rev.* **1998**, *27*, 289; C. A. Schalley, A. Lützen, M. Albrecht, *Chem. Eur. J.* **2004**, *10*, 1072.
[10] V. Amendola, L. Fabbrizzi, L. Gianelli, C. Maggi, C. Mangano, P. Pallavicini, M. Zema, *Inorg. Chem.* **2001**, *40*, 3579.
[11] See, for example: G. S. Hanan, D. Volkmer, U. S. Schubert, J.-M. Lehn, G. Baum, D. Fenske, *Angew. Chem.* **1997**, *109*, 1929; *Angew. Chem. Int. Ed. Engl.* **1997**, *36*, 1842; P. N. W. Baxter, J.-M. Lehn, B. O. Kneisel, D. Fenske, *Chem. Commun.* **1997**, 2231.
[12] A. Petitjean, N. Kyritsakas, J.-M. Lehn, *Chem. Commun.* **2004**, 1168.
[13] Part of this work has appeared as a preliminary communication: L. H. Uppadine, J.-M. Lehn, *Angew. Chem.* **2004**, *116*, 242; *Angew. Chem. Int. Ed.* **2004**, *43*, 240.
[14] J. Chesterfield, J. F. W. McOmie, E. R. Sayer, *J. Chem. Soc.* **1955**, 3478.
[15] J. J. Wade (Riker Laboratories Inc. (US)), European Patent Application EP0121341, **1984**.
[16] The coordination reaction between $Co^{II}(OAc)_2{\cdot}4H_2O$ and pyridine-2-aldehyde-2′-pyridylhydrazone also results in deprotonation of the ligand with concomitant oxidation of Co^{II} to Co^{III}: F. Lions, K. V. Martin, *J. Am. Chem. Soc.* **1958**, *80*, 3858.
[17] The Fe^{II} complex of deprotonated pyridine-2-aldehyde-2′-pyridylhydrazone has a high stability constant ($\log\beta_2 = 33$ in aqueous solution), approximately double that of the protonated complex ($\log\beta_2 = 16.7$): R. W. Green, P. S. Hallman, F. Lions, *Inorg. Chem.* **1964**, *3*, 376.
[18] Addition of DCl in D_2O (2.49 M, 10 μL) to a solution of green corner complex **13** (4.98 mo μl) in 4:1 $[D_3]MeCN/D_2O$ (500 μL) gave a red solution with a diamagnetic ^1H NMR spectrum. The pronounced colour change green→red can therefore be associated with deprotonated and protonated versions of **13**, respectively. The protonation state of **13** does not affect the spin state of the iron(II) centre.
[19] For a discussion on the acid–base equilibria of transition-metal complexes containing tridentate heterocyclic hydrazone ligands, see reference [17] and also: J. F. Geldard, F. Lions, *Inorg. Chem.* **1963**, *2*, 270; T. Taya, Y. Mukouyama, K. Doi, M. Otomo, *Bull. Chem. Soc. Jpn.* **1994**, *67*, 710.
[20] Similarly, Fe^{II} can be coordinated to protonated or deprotonated pyridine-2-aldehyde-2′-pyridylhydrazone (PAPHY) without further oxidation to Fe^{III}, whereas Co^{II} spontaneously oxidises to Co^{III} when reacted with PAPHY (see ref. [17]).
[21] B. N. Figgis, E. S. Kucharski, A. H. White, *Aust. J. Chem.* **1983**, *36*, 1563.
[22] K. M. Gardinier, R. G. Khoury, J.-M. Lehn, *Chem. Eur. J.* **2000**, *6*, 4124.
[23] M. L. Scudder, H. A. Goodwin, I. G. Dance, *New J. Chem.* **1999**, *23*, 695.
[24] H. Sleiman, P. N. W. Baxter, J.-M. Lehn, K. Airola, K. Rissanen, *Inorg. Chem.* **1997**, *36*, 4734.
[25] a) E. C. Constable, G. Baum, E. Bill, R. Dyson, R. van Eldik, D. Fenske, S. Kaderli, D. Morris, A. Neubrank, M. Neuburger, D. R. Smith, K. Wieghardt, M. Zehnder, A. D. Zuberbühler, *Chem. Eur. J.* **1999**, *5*, 498; b) A. T. Baker, H. A. Goodwin, *Aust. J. Chem.* **1985**, *38*, 207.
[26] D. Onggo, J. M. Hook, D. Rae, H. A. Goodwin, *Inorg. Chim. Acta* **1990**, *173*, 19.
[27] For a review on the NMR of paramagnetic substances, see: I. Bertini, C. Luchinat, *Coord. Chem. Rev.* **1996**, *150*, 1.
[28] For examples of the ^1H NMR spectra of cobalt(II) 2,2′:6′,2″-terpyridine complexes, see: E. C. Constable, C. E. Housecroft, T. Kulke, C. Lazzarini, E. R. Schofield, Y. Zimmermann, *J. Chem. Soc. Dalton Trans.* **2001**, 2864; E. C. Constable, T. Kulke, M. Neuburger, M. Zehnder, *New J. Chem.* **1997**, *21*, 1091; G. D. Storrier, S. B. Colbran, D. C. Craig, *J. Chem. Soc. Dalton Trans.* **1998**, 1351.
[29] J. Rojo, F. J. Romero-Salguero, J.-M. Lehn, G. Baum, D. Fenske, *Eur. J. Inorg. Chem.* **1999**, 1421.
[30] a) J. Fleisch, P. Gütlich, K. M. Hasselbach, W. Müller, *J. Phys. Colloq.* **1974**, *C6*, 659, Supplement au No 12; b) Sohrin, H. Kokusen, M. Matsui, *Inorg. Chem.* **1995**, *34*, 3928; c) K. A. Reeder, E. V. Dose, L. J. Wilson, *Inorg. Chem.* **1978**, *17*, 1071; d) J. D. Crane, J.-P. Sauvage, *New J. Chem.* **1992**, *16*, 649; e) D. Onggo, H. A. Goodwin, *Aust. J. Chem.* **1991**, *44*, 1539.
[31] P. Gütlich, *Struct. Bonding* **1981**, *44*, 83; D. J. Hathcock, K. Stone, J. Madden, S. J. Slattery, *Inorg. Chim. Acta* **1998**, *282*, 131; T. Ayers, S. Scott, J. Goins, N. Caylor, D. Hathcock, S. J. Slattery, D. L. Jameson, *Inorg. Chim. Acta* **2000**, *307*, 7.
[32] M. Enamullah, W. Linert, V. Gutmann, R. F. Jameson, *Monatsh. Chem.* **1994**, *125*, 1301.
[33] M. Yamada, M. Ooidemizu, Y. Ikuta, S. Osa, N. Matsumoto, S. Iijima, M. Kojima, F. Dahan, J.-P. Tuchagues, *Inorg. Chem.* **2003**, *42*, 8406; G. A. Renovitch, W. A. Baker Jr., *J. Am. Chem. Soc.* **1967**, *89*, 6377.
[34] L. H. Uppadine, G. Rogez, J.-M. Lehn, unpublished results.
[35] B. Chiswell, J. F. Geldard, A. T. Phillip, F. Lions, *Inorg. Chem.* **1964**, *3*, 1272.
[36] P. S. Braterman, J.-I. Song, R. D. Peacock, *Inorg. Chem.* **1992**, *31*, 555; G. S. Heath, L. J. Yellowlees, P. S. Braterman, *J. Chem. Soc. Chem. Commun.* **1981**, 287.
[37] J. B. Flanagan, S. Margel, A. J. Bard, F. C. Anson, *J. Am. Chem. Soc.* **1978**, *100*, 4248.
[38] G. Denti, S. Campagna, L. Sabatino, S. Serroni, M. Ciano, V. Balzani, *Inorg. Chem.* **1990**, *29*, 4750.
[39] J. M. Rao, D. J. Macero, M. C. Hughes, *Inorg. Chim. Acta* **1980**, *41*, 221.
[40] A. M. Bond, A. F. Hollenkamp, S. B. Thompson, A. R. Bourne, P. A. Huf, T. G. Watson, *Anal. Chem.* **1988**, *60*, 1023; E.-C. Liu, M. R. Van De Mark, *J. Chem. Soc. Chem. Commun.* **1982**, 1176.
[41] T. Ayers, R. Turk, C. Lane, J. Goins, D. Jameson, S. J. Slattery, *Inorg. Chim. Acta* **2004**, *357*, 202.
[42] The one-electron oxidation process $Co^{II} \rightarrow Co^{III} + e^-$ is considered less likely, since this does not account for the four electron oxidation in grid **3** and because the cobalt(IV) oxidation state is relatively rare (see R. D. Webster, G. A. Heath, A. M. Bond, *J. Chem. Soc. Dalton Trans.* **2001**, 3189; K. Dimitrou, A. D. Brown, T. E. Concolino, Al L. Rheingold, G. Christou, *Chem. Commun.* **2001**, 1284; F. C. Anson, T. J. Collins, R. J. Coots, S. L. Gipson, T. G. Richmond, *J. Am. Chem. Soc.* **1984**, *106*, 5037).
[43] O. A. Gansow, R. J. Olcott, R. H. Holm, *J. Am. Chem. Soc.* **1967**, *89*, 5470; T. A. James, J. A. McCleverty, E. D. McKenzie, R. D. Moore, *Inorg. Chim. Acta* **1985**, *101*, 113.
[44] Solid-state magnetic studies on grid **1** show that the two Co^{II} ions are high spin over the temperature range from 350 K to 5 K (L. H. Uppadine, G. Rogez, J.-M. Lehn, unpublished results).
[45] J. C. Yoder, J. P. Roth, E. M. Gussenhoven, A. S. Larsen, J. M. Mayer, *J. Am. Chem. Soc.* **2003**, *125*, 2629; D. J. Szalda, C. Creutz, D. Mahajan, N. Sutin, *Inorg. Chem.* **1983**, *22*, 2372.
[46] C. Piguet, G. Bernardinelli, B. Bocquet, O. Schaad, A. F. Williams, *Inorg. Chem.* **1994**, *33*, 4112; L. J. Charbonnière, A. F. Williams, C. Piguet, G. Bernardinelli, E. Rivara-Minten, *Chem. Eur. J.* **1998**, *4*, 485.
[47] B. S. Brunschwig, C. Creutz, D. H. Macartney, T. K. Sham, N. Sutin, *Faraday Discuss. Chem. Soc.* **1982**, *74*, 113.
[48] J. McCrea, V. McKee, T. Metcalfe, S. S. Tandon, J. Wikaira, *Inorg. Chim. Acta* **2000**, *297*, 220.
[49] For examples of the effect of ligand protonation state on the Fe^{III}/Fe^{II} redox couple, see: C. Brewer, G. Brewer, C. Luckett, G. S. Marbury, C. Viragh, A. M. Beatty, W. R. Scheidt, *Inorg. Chem.* **2004**, *43*, 2402; F. Lambert, C. Policar, S. Durot, M. Cesario, L. Yuwei, H. Korri-Youssoufi, B. Keita, L. Nadjo, *Inorg. Chem.* **2004**, *43*, 4178;

R. F. Carina, L. Verzegnassi, G. Bernardinelli, A. F. Williams, *Chem. Commun.* **1998**, 2681; Y. Sunatsuki, H. Ohta, M. Kojima, Y. Ikuta, Y. Goto, N. Matsumoto, S. Iijima, H. Akashi, S. Kaizaki, F. Dahan, J.-P. Tuchagues, *Inorg. Chem.* **2004**, *43*, 4154.
[50] D. B. Harden, M. J. Mokrosz, L. Strekowski, *J. Org. Chem.* **1988**, *53*, 4137.
[51] G. Gritzner, J. Kuta, *Pure Appl. Chem.* **1984**, *56*, 461.
[52] F. Ammar, J. M. Savéant, *J. Electroanal. Chem. Interfacial Electrochem.* **1973**, *47*, 215; R. L. Myers, I. Shain, *Anal. Chem.* **1969**, *41*, 980.
[53] J. Bley-Escrish, J. P. Gisselbrecht, E. Vogel, M. Gross, *Eur. J. Inorg. Chem.* **2002**, 2829.
[54] "Processing of X-ray Diffraction Data Collected in Oscillation Mode": Z. Otwinowski, W. Minor, *Methods Enzymol.* **1997**, *276*, 307.
[55] G. M. Sheldrick, SHELXS, Universität Göttingen, Göttingen (Germany), **1997**.
[56] G. M. Sheldrick, SHELXL-97, Program for the Refinement of Crystal Structures, Universität Göttingen, Göttingen (Germany), **1997**.
[57] L. J. Farrugia, *J. Appl. Crystallogr.* **1999**, *32*, 837.
[58] B. V. Nonius, OpenMolen, *Interactive Structure Solution*, Delft (The Netherlands), **1997**.
[59] D. T. Cromer, J. T. Waber, *International Tables for X-ray Crystallography*, *Vol. IV*, Kynoch, Birmingham, **1974**.
[60] G. M. Sheldrick, *Acta Crystallogr. Sect. A* **1990**, *46*, 467.
[61] A. L. Spek, PLATON, A Multipurpose Crystallographic Tool, Utrecht University, Utrecht (The Netherlands), **1998**.

Received: November 30, 2004
Published online: February 24, 2005

